Molecular Therapy
Original Article

Local Immunomodulation with Anti-inflammatory Cytokine-Encoding Lentivirus Enhances Functional Recovery after Spinal Cord Injury

Jonghyuck Park,[1] Joseph T. Decker,[1] Daniel J. Margul,[1,2] Dominique R. Smith,[1] Brian J. Cummings,[3] Aileen J. Anderson,[3] and Lonnie D. Shea[1,4]

[1]Department of Biomedical Engineering, University of Michigan, Ann Arbor, MI 48105, USA; [2]Department of Biomedical Engineering, Northwestern University, Evanston, IL 60208, USA; [3]Department of Anatomy and Neurobiology, University of California, Irvine, Irvine, CA 92697, USA; [4]Department of Chemical Engineering, University of Michigan, Ann Arbor, MI 48105, USA

Trauma to the spinal cord and associated secondary inflammation can lead to permanent loss of sensory and motor function below the injury level, with the resulting environment serving as a barrier that limits regeneration. In this study, we investigate the localized expression of anti-inflammatory cytokines IL-10 and IL-4 via lentiviral transduction in multichannel bridges. Porous multichannel bridges provide physical guidance for axonal outgrowth with the cytokines hypothesized to modulate the neuroinflammatory microenvironment and enhance axonal regeneration. Gene expression analyses indicated that induced IL-10 and IL-4 expression decreased expression of pro-inflammatory genes and increased pro-regenerative genes relative to control. Moreover, these factors led to increased numbers of axons and myelination, with approximately 45% of axons myelinated and the number of oligodendrocyte myelinated axons significantly increased by 3- to 4-fold. Furthermore, the combination of a bridge with IL-10 and IL-4 expression improved locomotor function after injury to an average score of 6 relative to an average score of 3 for injury alone. Collectively, these studies highlight the potential for localized immunomodulation to decrease secondary inflammation and enhance regeneration that may have numerous applications.

INTRODUCTION

Trauma to the spinal cord creates an initial injury, with secondary inflammatory responses further exacerbating the damage. Secondary events can include ischemia, anoxia, and excitotoxicity for the first minutes, hours, and days after injury. These events create an inhibitory microenvironment and damage adjacent intact tissue, resulting in permanent loss of motor and sensory functions below the level of the injury.[1–4] Activated macrophages and neutrophils release pro-inflammatory cytokines, which induce reactive astrocytes contributing to increase the secretion of inhibitory molecules such as chondroitin sulfate proteoglycans (CSPGs) at the injury site.[4,5] An inflammatory response at the injured spinal cord leads to swelling and thus compression within the vertebral column and secondary damage.[4–7] Moreover, reactive astrocytes form a glial scar at the lesion over time, which acts as a mechanical and chemical barrier for axonal regrowth.

While inflammation can induce damage, the presence of macrophages is also necessary for regeneration.[5,8–10] The regenerative function of macrophages may be associated with distinct subsets, which are derived from both resident microglia and hematogenous macrophages. Macrophages have plasticity that depends on the microenvironment, and the phenotypes have been described as ranging from pro-inflammatory M1 (or classically activated) to pro-regenerative M2 (or alternatively activated). Although many argue that the phenotypes are not binary, these designations provide a useful frame of reference for analysis.[10–12] The pro-inflammatory phenotype is induced by prototypical T helper 1 (T_H1) cytokines such as interferon-γ (IFNγ), which induce pro-inflammatory cytokines, reactive oxygen species (ROS), and nitric oxide (NO), all of which contribute to inflammation and tissue damage. By contrast, the pro-regenerative phenotype is derived from T_H2 cytokines including interleukin (IL)-4, IL-10, and IL-13.[10–13] These anti-inflammatory cytokines contribute to wound healing and tissue repair, and enhance regrowth of axons against a myelin inhibitory environment in a spinal cord injury (SCI).[11–13]

Poly(lactide-co-glycolide) (PLG) has been widely used for nerve tissues repair because of biodegradation characteristics and ease of processing.[14] We have previously reported that PLG multichannel bridges, which provide a structural conduit across the injury site, have been employed to promote axonal regrowth through the bridge after SCI.[15–17] The presence of the bridge supports host cell infiltration, which helps reduce the extent of glial scar formation and astrogliosis.[17–19] In addition, localized expression of trophic factors via

Received 19 January 2018; accepted 23 April 2018;
https://doi.org/10.1016/j.ymthe.2018.04.022.

Correspondence: Lonnie D. Shea, Department of Biomedical Engineering, University of Michigan, 2200 Bonisteel Boulevard, 1119 Carl A. Gerstacker Building, Ann Arbor, MI 48109-2099, USA.
E-mail: ldshea@umich.edu

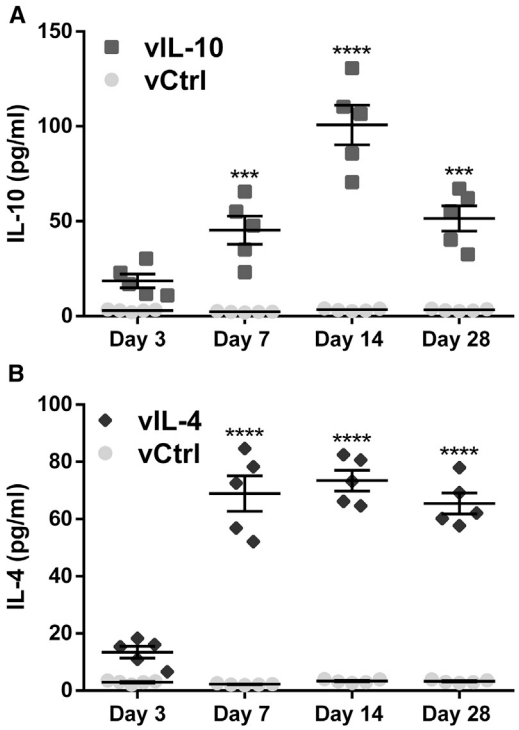

Figure 1. Delivered Anti-inflammatory Cytokines from Multichannel Bridge Transduce *In Vivo* Host Cells and Promote a Sustained Release of Transgenes

The protein expression levels from spinal cord were quantified by ELISA as a function of time. The expression levels of protein started to increase significantly at day 7 post-SCI compared with vCtrl in both (A) vIL-10 and (B) vIL-4 delivery groups. A two-way ANOVA followed by Šidák correction for the multiple comparisons, ***$p < 0.001$, ****$p < 0.0001$, compared with vCtrl (mean ± SEM, n = 5/group).

bridges has been able to alter the post-SCI microenvironment and enhance the number of regenerating axons and the extent of myelination.[9,15,20] Collectively, the results have indicated the potential to support regeneration through the injury, which has contributions from a modestly attenuated inflammatory response. Nevertheless, the multichannel bridge alone is limited in its capability to enhance functional regeneration after SCI. Furthermore, the secondary inflammatory response remains and contributes to cell death and axonal retraction that may limit regeneration; thus, reducing this inflammation combined with inducing a pro-regenerative response may further enhance regeneration.

In the present study, we investigated nerve regeneration after SCI following local immunomodulation using lentiviral vector delivery of human anti-inflammatory cytokines IL-10 and IL-4 from a multichannel PLG bridge (Figure S1). We have previously demonstrated that lentiviral vectors have been successfully employed to transduce cell types commonly found following SCI, such as macrophages, Schwann cells, and fibroblasts.[9,15,21] IL-10 and IL-4 were investigated because of their dual neuroprotective and neuroregenerative abilities.[22–25] We hypothesized that the architectural aspects of the bridge would synergize with the immunomodulation provided by cytokines to attenuate inflammation and promote regeneration. A lateral hemisection model was employed for bridge implantation, and the inflammatory response was characterized histologically, and through transcriptome analysis for inflammatory and regenerative gene expression. The number of axons and their extent of myelination were characterized histologically, with locomotor tests performed for functional recovery.

RESULTS

Transgene Expression after Anti-inflammatory Cytokine Delivery

Local transgene expression by delivery of human IL-10 encoding lentiviral vector (vIL-10) and IL-4 encoding lentiviral vector (vIL-4) from spinal cord tissues was quantified over time, with firefly luciferase encoding lentivirus used as a control (vCtrl) (Figure 1). By day 7, IL-10 and IL-4 protein expression levels were significantly increased relative to vCtrl (45.3 ± 8.4 versus 5.4 ± 0.1 pg/mL, $p < 0.001$, and 68.9 ± 6.2 versus 5.4 ± 0.1 pg/mL, $p < 0.0001$, respectively), with elevated levels maintained through at least 28 days post-SCI. IL-10 and IL-4 protein levels at day 3 trended greater than control (18.6 ± 4.7 versus 6.8 ± 0.1 pg/mL, $p > 0.05$, and 13.5 ± 2.6 versus 6.8 ± 0.1 pg/mL, $p > 0.05$, respectively), yet lentiviral expression required multiple days to achieve protein levels above background. IL-10 expression increased through day 14 and then declined at day 28, yet was still significantly above control (51.4 ± 7.2 versus 6.1 ± 0.1 pg/mL; $p < 0.001$) (Figure 1A). Conversely, IL-4 levels were maximal at day 7 and persisted through the 28 days of this study (65.5 ± 6.7 versus 6.1 ± 0.1 pg/mL; $p < 0.0001$) (Figure 1B).

Anti-inflammatory Cytokines Modulate Microenvironment after SCI

We investigated alteration in the transcriptome caused by anti-inflammatory factors through cDNA microarray at day 7 post-SCI (Figure 2A). A total of 24,581 genes were measured. A total of 368 transcripts for the vIL-10 condition and 132 transcripts for the vIL-4 condition were upregulated 2-fold or greater. An additional 391 transcripts in the vIL-10 condition and 92 transcripts in the vIL-4 condition were downregulated more than 2-fold. We sought to identify patterns among these genes that differentiated the vIL-10 and vIL-4 conditions from the vCtrl to gain insight into the active biological processes at all conditions. We were primarily interested in ontologies that overlapped between the two cytokine conditions compared with vCtrl; 10 representative ontologies that were significant in both conditions are presented in Figures 2B and 2C. Gene ontology (GO) analysis for genes that were 2-fold downregulated primarily identified ontologies associated with neuroinflammation responses (e.g., immune response; Figure 2D; Figures S2A–S2D). Real-time qPCR was used to confirm these results (Figure 2F). The results agreed broadly with the microarray data at day 7; then gene expression showed a decrease in response to vIL-10 and vIL-4. Conversely, upregulated genes matched to ontologies related to the functional recovery (e.g., chemical synaptic transmission; Figure 2E;

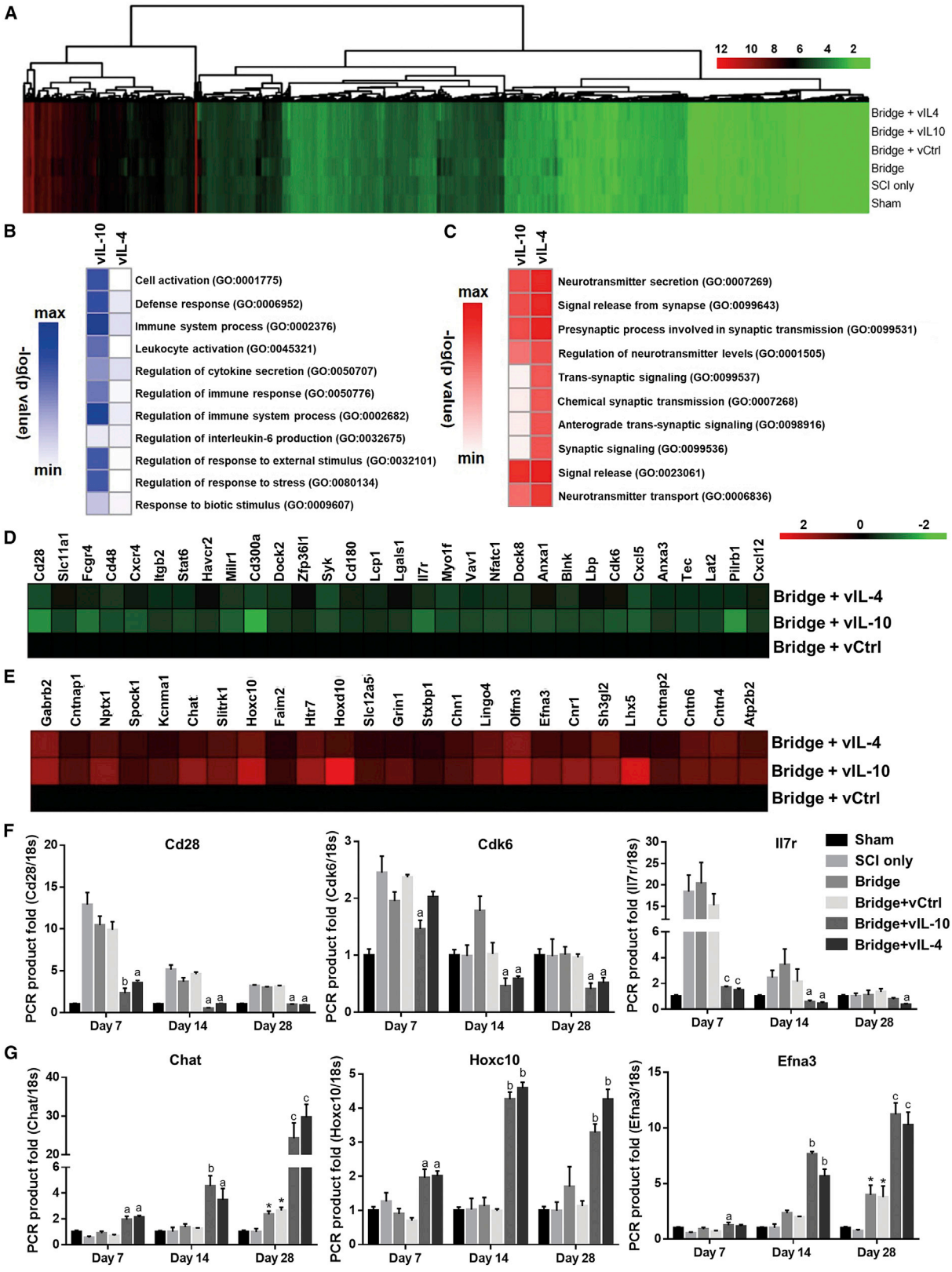

(legend on next page)

Figures S2E and S2F). We confirmed these results via real-time qPCR of genes in these over-represented pathways. Time-course measurements showed an increase in transcript quantity further out from the time of injury (day 14 or 28) along with a modest upregulation at day 7 in response to anti-inflammatory factors, which corresponds with the microarray data (Figure 2G).

Anti-inflammatory Cytokines Induce Macrophage Polarization

We investigated macrophage polarization by cytokine expression, because macrophages are central players in the inflammatory response following SCI (Figure 3). Initially, the gene expression profiles associated with M1 and M2 phenotypes were assessed through microarray and real-time qPCR. M1 markers levels were the same or downregulated in vIL-10 and vIL-4 relative to vCtrl. In contrast, M2 genes levels were upregulated in response to vIL-10 and vIL-4 compared with vCtrl (Figure 3A). Based on the microarray, subsets of M1 and M2 genes were validated using real-time qPCR over time (Figures 3B and 3C). The results agreed broadly with the microarray at day 7; then the expression levels of inflammation markers *Cd86*, major histocompatibility complex (MHC) class II (*MHC-II*), and inducible nitric oxide synthase (*iNOS*) were significantly decreased in vIL-10 and vIL-4 relative to vCtrl, while anti-inflammatory markers *Cd206*, resistin-like alpha (*Retnla*), and arginase 1 (*Arg1*) were substantially increased in anti-inflammatory delivery groups over time. Subsequently, immunofluorescence staining was performed to confirm and quantify the densities of total macrophages ($Hoechst^+/F4/80^+$) and macrophages expressing the M2-associated factor Arg1 ($Hoechst^+/F4/80^+/ Arg1^+$) (Figures 3D–3G) at the site of injury. In agreement with previous study,[21] no statistical differences were observed in the density of macrophages within the bridge at days 14 and 28 for all conditions (Figure 3H); however, the number of macrophages expressing Arg1 was substantially increased in anti-inflammatory cytokine groups relative to bridge only and vCtrl groups (Figure 3I). Furthermore, the level of anti-inflammatory cytokines was associated with the number of M2 phenotypes (Figure S3). These data indicated that overexpression of anti-inflammatory factors influences macrophage polarization at the injury.

Anti-inflammatory Factors Promote Axonal Regrowth and Remyelination

We next assessed the impact of anti-inflammatory cytokine expression on axonal regrowth and remyelination in the sub-acute (28 days) and chronic (84 days) phase after SCI (Figures 4 and 5). Initially, the microarray results were analyzed for alteration in the expression of neuronal development-associated ontologies (e.g., neural system development and neuron differentiation ontologies) (Figure 4A; Figure S2E). The results demonstrated more than 2-fold upregulation of associated gene expression in the vIL-10 and vIL-4 conditions compared with vCtrl. We also confirmed expression levels for selected genes associated with neural system development. As a transcriptional regulator, LIM homeobox 5 (*Lhx5*) is involved in the control of differentiation and development of motor neurons.[26] Hyaluronan and proteoglycan link protein 4 (*Hapln4*) is a key molecule for neuronal functions and saltatory conduction,[27] and transient receptor potential channel subfamily C (*Trpc5*) plays a role in the induction of the differentiation of neural progenitor cells.[28] Real-time qPCR results indicate increased and persistent expression through the 28 days in vIL-10 and vIL-4 groups, consistent with the microarray studies (Figure 4B).

Subsequently, we investigated axonal regrowth and myelination after SCI via immunofluorescence for myelin basic protein (MBP), myelin protein zero (P0), and neurofilament 200 (NF200). Coronal sections were grouped by dividing the bridge based on three regions: rostral, middle, and caudal (Figure S1C). The data revealed that $NF200^+$ axons were observed throughout the bridges in the sub-acute phase (Figures 4C–4F). At the rostral position, delivery of lentivirus encoding either IL-10 or IL-4 substantially increased axon number relative to the empty bridge and vCtrl groups at day 28 post-bridge implantation (Figure 4G). The number of axons at the middle and caudal sections of the bridge were less than the number observed for the rostral region. However, for the caudal location, the number of axons in anti-inflammatory groups was significantly increased compared with empty bridge and vCtrl groups, while the axon numbers in the middle position for all conditions reached similar levels at day 28 post-SCI (Figures 4H and 4I). MPB myelinated ($NF200^+/MBP^+$) axons were also seen within the bridge, where regenerating axons were present. The middle and caudal locations showed decreased levels of MBP^+ axons compared with the rostral position, while both IL-10 and IL-4 expression bridges resulted in greater MBP^+ axon counts relative to empty bridge and vCtrl groups for the caudal locations (Figures 4G–4I). The number of Schwann cell-derived myelinated axons ($NF200^+/MBP^+/P0^+$) was significantly increased in anti-inflammatory delivery groups only at the rostral location. Generally, MPB myelinated axons were seen in the center of bridges or midline of spinal cord (channels 2, 5, and 6 in Figure S1A), while Schwann cell-derived axons were observed around the outer edges of the bridge (Figures S4A and S4B). Even though the number of MBP^+ axons was greatest for the vIL-10 and vIL-4 groups at rostral and caudal locations, no significant difference was obtained for the percentage of myelinated axons between conditions throughout the bridges (Figure S4C).

At day 84, analysis of immunofluorescence data indicated that regenerating axons were typically found throughout the bridge in bundles

Figure 2. Anti-inflammatory Cytokines Modulate Microenvironment after SCI

(A) Microarray data for spinal cord 7 days post-injury in all conditions. (B and C) Ten representative significant ontologies for both vIL-10 and vIL-4 from genes downregulated (B) or upregulated (C) more than 2-fold from vCtrl. Gene ontology (GO) accession numbers were also presented. As examples, (D) downregulated genes associated with immune system process (GO: 0002682) in the leukocyte activation gene ontology, and (E) upregulated genes associated with chemical synaptic transmission (GO: 0007268) ontology were presented. (F and G) Real-time qPCR for selected genes from the immune system process (F), and the chemical synaptic transmission (G) ontologies over time. A two-way ANOVA with Tukey's post hoc test for the multiple comparisons. $^a p < 0.05$, $^b p < 0.01$, and $^c p < 0.001$ compared with vCtrl, and $^* p < 0.05$ compared with SCI only (mean ± SEM, n = 5–6/group and time point).

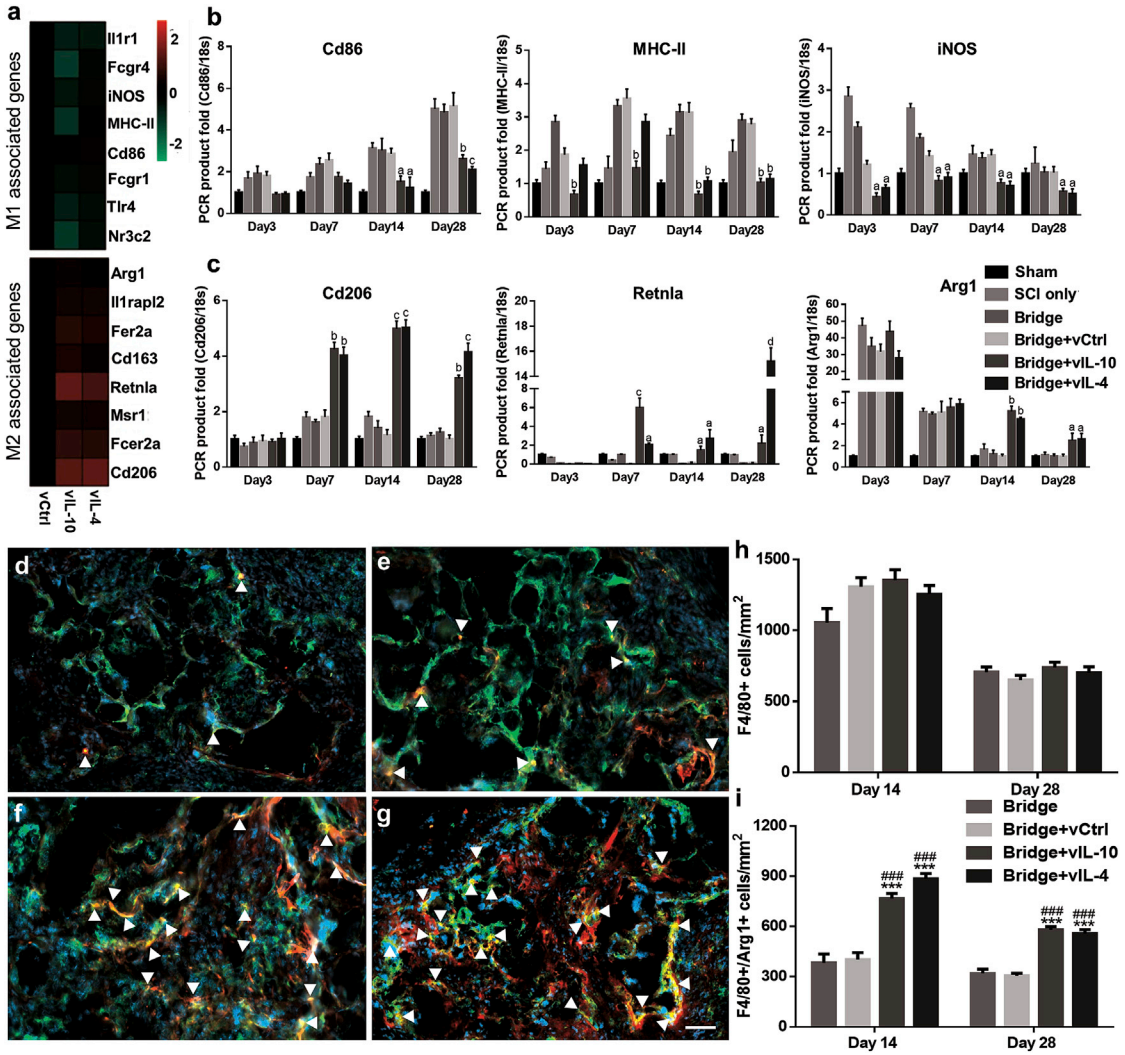

Figure 3. Anti-inflammatory Cytokines Control Macrophage Activation, Differentiation, and Polarization

(A) cDNA microarray heatmaps show clustering of M1- and M2-associated genes at day 7 post-SCI. (B and C) Real-time qPCR confirms increase or decrease in selected (B) M1 and (C) M2 markers as a function of time. (D–G) Immunodetection of F4/80$^+$/arginase$^+$/Hoechst$^+$ macrophages (yellow, white arrowheads) in (D) empty bridge, (E) bridge+vCtrl, (F) bridge+vIL-10, and (G) bridge+vIL-4 group at day 14 post-SCI (scale bar, 50 μm). (H) The density of total F4/80$^+$ macrophages at 14 and 28 days post-SCI within the bridge. (I) The density of M2 macrophages (F4/80$^+$/arginase1$^+$/Hoechst$^+$). A two-way ANOVA followed by Tukey's post hoc test where $^a p < 0.05$, $^b p < 0.01$, $^c p < 0.001$, and $^d p < 0.0001$ compared with vCtrl for real-time qPCR; $^{***} p < 0.001$ compared with vCtrl; and $^{\#\#\#} p < 0.001$ compared with Bridge only for immunofluorescence (mean ± SEM, n = 5–6/group and time point).

of two or more axons in the anti-inflammatory cytokine groups (Figures 5A and 5B), which was consistent with previous reports.[9,18] The total number of NF200$^+$ axons was significantly increased in the anti-inflammatory cytokine groups relative to bridge only and vCtrl (Figure 5C). Moreover, a greater number of NF200$^+$ axons was observed at day 84 relative to day 28 for all conditions (Figure S5). Similar to axon number, myelinated axons (NF200$^+$/MBP$^+$) were also significantly increased in vIL-10 and vIL-4 delivery groups by 3- to 4-fold compared with bridge only and vCtrl, and approximately 45% and 44% of the NF200$^+$ axons were myelinated with vIL-10 and vIL-4 delivery (Figures 5C and 5D).

In addition to axonal regrowth and myelination, we also evaluated the source of myelination in the chronic phase (Figures 5E and 5F). The significantly greater number of oligodendrocyte-derived myelinated axons (NF200$^+$/MBP$^+$/P0$^-$) was seen in anti-inflammatory cytokine groups relative to bridge only and vCtrl. About 48% and 52% of myelinated axons were ensheathed by oligodendrocyte-derived myelin in vIL-10 and vIL-4, respectively. Moreover, a greater number of oligodendrocyte-derived myelin was observed at day 84 relative to day 24 for the vIL-10 and vIL-4 groups (Figures S5C and S5D). However, there were no significant differences in Schwann cell-mediated myelination (Figure S5). Collectively, these data demonstrate that

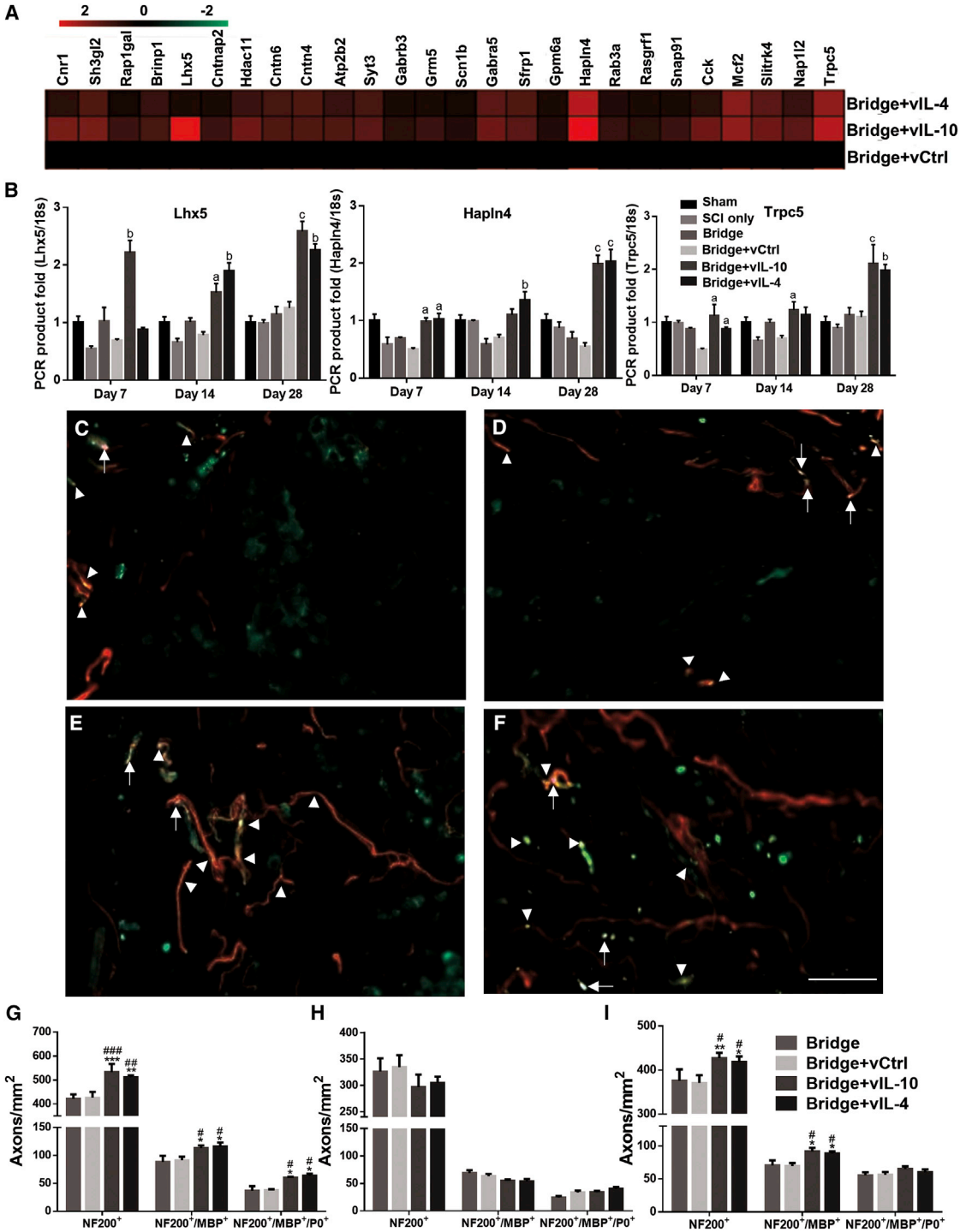

Figure 4. Axonal Regrowth and Remyelination in the Sub-acute Phase of SCI by Anti-inflammatory Cytokines

(A and B) The alterations of neural system development (GO:0007399)-associated gene expression was investigated via microarray and real-time qPCR. Tissue sections were stained using NF200 (axons), an anti-myelin basic protein (MBP) (all myelin), and myelin protein zero (P0) (Schwann cell-derived myelination). Immunofluorescence of myelinated total axons ($NF200^+/MBP^+/P0^+$) with (C) empty bridge, (D) vCtrl, (E) vIL-10, or (F) vIL-4 delivery at the rostral location (scale bar, 30 μm). White arrowheads indicate all myelinated axons ($NF200^+/MBP^+$), and white arrows show myelinated axons by Schwann cells ($NF200^+/MBP^+/P0^+$). (G–I) Quantification of total number of axons,

(legend continued on next page)

the localized expression of anti-inflammatory cytokines, combined with a more permissive microenvironment of the multichannel bridge, promotes axonal regeneration and axonal remyelination as a function of time.

Anti-inflammatory Factors Improve Functional Recovery after SCI

cDNA microarray heatmap revealed a 2-fold upregulation of functional recovery-associated ontologies in the anti-inflammatory cytokine groups relative to vCtrl (e.g., locomotor recovery and synapse organization ontologies) (Figure 6A; Figure S2F). Real-time qPCR analysis of selected functional recovery-associated genes indicated a significant increase within vIL-10 and vIL-4 groups relative to vCtrl, which was maintained until 28 days after SCI (Figure 6B). Subsequently, locomotor function was evaluated using the Basso Mouse Scale (BMS) before injury, at day 3, and then weekly for 84 days post-SCI (Figure 6C). Before SCI, all mice in all conditions were fully functional. At day 3 post-SCI, no movement was observed in ipsilateral hindlimb in any group, yet BMS scores gradually improved with time. The BMS score in vIL-10 and vIL-4 groups indicated a significantly enhanced recovery of motor function compared with vCtrl starting at day 14 through day 84 after SCI. In addition, the bridge only and vCtrl groups substantially improved their motor function relative to the SCI only group from day 63 post-SCI. Specific aspects of locomotor recovery in mice after SCI do not follow a typical recovery pattern and are thus not reflected in the overall BMS score.[29] Therefore, BMS subscoring was performed after day 63 to analyze specific components of locomotion recovery between groups[30,31] (Figure S6). The subscoring indicated that both vIL-10 and vIL-4 delivery substantially improved stepping frequency, paw position, forelimb and hindlimb coordination, tail position, and trunk stability compared with vCtrl. Furthermore, in agreement with BMS score, the subscore for the bridge only and vCtrl was greater than that in SCI only, suggesting that the implanted multichannel bridge itself also has a positive effect on locomotor functional recovery after SCI. These data demonstrate that localized expression of the anti-inflammatory factors and multichannel bridge increased motor function following injury.

DISCUSSION

The injured microenvironment cues favor differentiation of macrophage into M1 phenotypes; also, persistent induction of pro-inflammatory cytokine expression was observed.[5,8,32,33] Conversely, anti-inflammatory cytokines necessary for inducing M2 phenotype or attenuating macrophage function were unchanged or decreased.[8,32,33] We report that localized delivery of anti-inflammatory cytokines encoding lentivirus can modulate the local neuroinflammatory microenvironment and induce M2-favored conditions at the injury. cDNA microarray showed that neuroinflammatory-related genes levels were decreased more than 2-fold relative to vCtrl, while upregulation of synaptogenesis- and neurogenesis-related gene expression was observed in both vIL-10 and vIL-4 groups (Figure 2; Figure S2). Real-time qPCR indicated that anti-inflammatory cytokines downregulated inflammatory response-associated expression such as *MHC-II*, *iNOS*, and *Cd86* relative to vCtrl throughout day 28 post-SCI. As key markers of pro-inflammatory phenotype, these factors are associated with the initiation of immune responses and induce the release of pro-inflammatory factors, leading to an inhibitory microenvironment.[10,11] IL-10 and IL-4 also resulted in upregulation of anti-inflammatory markers such as *Arginase1*, *Cd206*, and *Retnla* at the injury. As markers of M2 macrophages, they enhance removal of apoptotic and necrotic cells, and attenuate release of pro-inflammatory factors, resulting in axonal regrowth and functional regeneration after SCI[12,21,32,34] (Figures 3A–3C). The transgene expression herein, and as also reported in a previous study, showed that delivered lentiviral vector started producing transgene at day 3 and was substantially increased at day 7 compared with control.[20,35] This may lead to significant alteration of gene expression profiles in vIL-10 and vIL-4 groups relative to vCtrl over time. Both IL-10 and IL-4 downregulate the secretion of pro-inflammatory factors after injury but via different pathways. Nuclear factor-κB (NF-κB) plays a critical role in the development of inflammation by regulating gene-encoding pro-inflammatory cytokines.[36] IL-10 has been shown to suppress NF-κB activation and its DNA binding through a STAT3-mediated pathway.[36,37] IL-4 utilizes a STAT6-mediated cascade, leading to expression of anti-inflammatory genes via suppression of IFNγ signaling.[24,38,39] In addition, IL-4 prevents production of inducible enzymes, which inhibit inflammatory factor-mediated NO synthesis, resulting in expression of anti-inflammatory factors.[40] Furthermore, glia cells express both IL-10 receptor and IL-4 receptor alpha (IL-4Rα) in the CNS, where IL-10 and IL-4 act as antagonists to inhibit secretion of pro-inflammatory factors from glia cells after injury.[22,23,25,39] In agreement with previous studies, Arg1 gene expression increased in all conditions and then returned to baseline at day 14, because microglia/macrophages have both M1 and M2 phenotypes early in the SCI.[32,41]

The local microenvironment modulation by anti-inflammatory cytokines controls macrophage activation, differentiation, and polarization (Figure 3). In the injured spinal cord, an analogous M1-to-M2 macrophage polarization as in normal tissue does not occur. As a function of time, M2 macrophages are decreased, while pathological M1 macrophages remain elevated at the injury site. Therefore, a transient and low number of pro-regenerative M2 macrophages in the damaged microenvironment may allow chronic inflammation and secondary damage after primary injury.[32,33] Although immunofluorescence showed a trend toward greater number of infiltrated F4/80$^+$ macrophages at day 14 post-SCI compared with empty bridge and vCtrl,

myelinated axons, and Schwann cell-derived myelinated axons at 28 days post-bridge implantation from the (G) rostral (300 μm), (H) middle (900 μm), and (I) caudal (1,600 μm) regions. For the statistical analysis, a two-way ANOVA with Tukey's post hoc test was used. $^{a}p < 0.05$, $^{b}p < 0.01$, and $^{c}p < 0.001$ compared with vCtrl for real-time qPCR (mean ± SEM, n = 5–6/group and time point); $^{*}p < 0.05$, $^{**}p < 0.01$, and $^{***}p < 0.001$ compared with vCtrl; and $^{\#}p < 0.05$, $^{\#\#}p < 0.01$, and $^{\#\#\#}p < 0.001$ relative to empty bridge for immunofluorescence (mean ± SEM, n = 5/group).

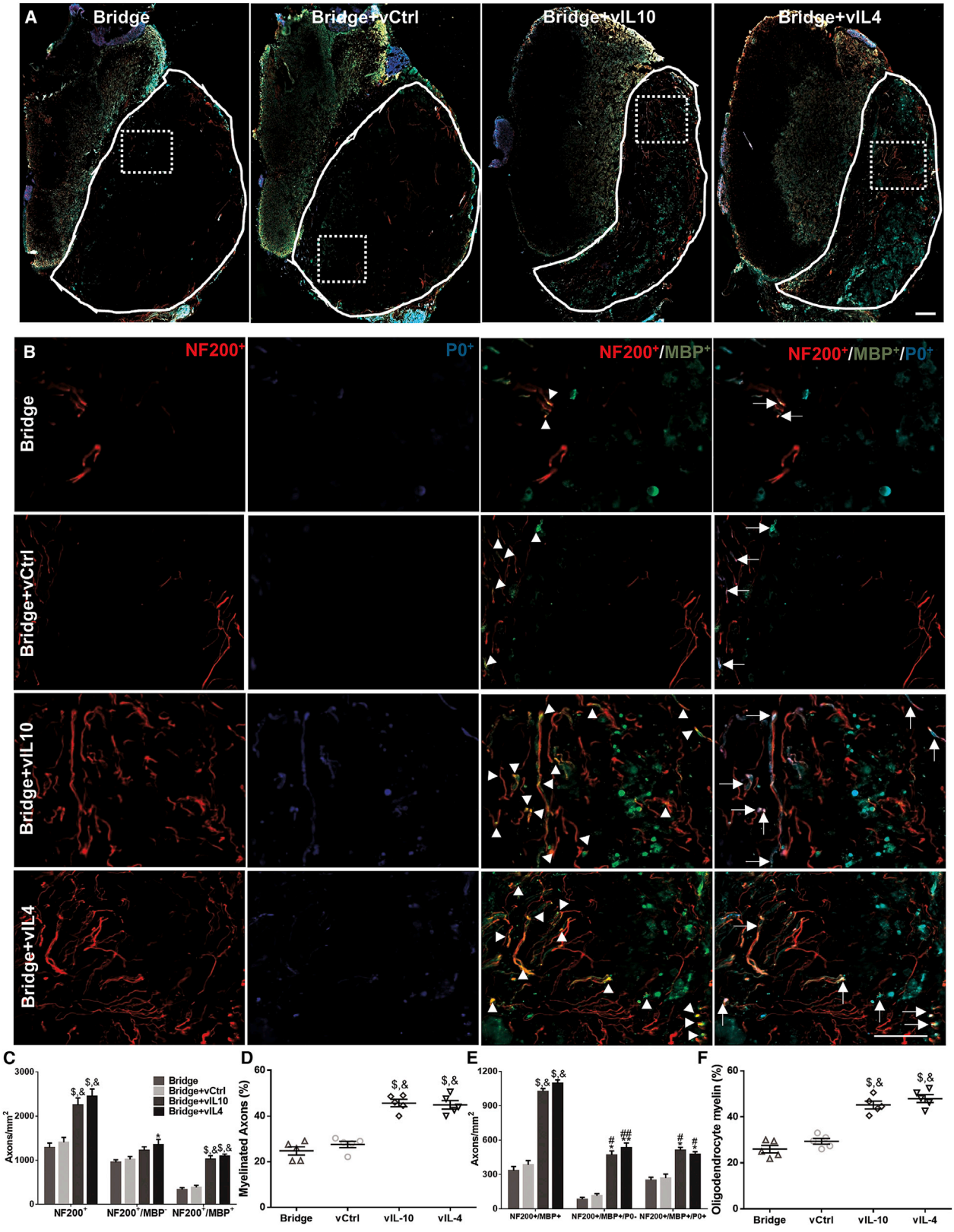

(legend on next page)

there were no significant changes between conditions. These observations are supported by prior reports that the infiltrating number of macrophages is known to peak around 7–10 days at the injured site and plateau for several days before decreasing.[8,21] More importantly, both vIL-10 and vIL-4 delivery significantly increased the number of M2 ($F4/80^+$/ $Arg1^+$) macrophages at days 14 and 28 relative to empty bridges and vCtrl. The increased number of $F4/80^+$/ $Arg1^+$ macrophages may be correlated with increased Arg1 levels and induction of an M2-favored microenvironment by IL-10 and IL-4 expression, because there is a linear trend between IL-10 and IL-4 expression and M2 numbers with a positive slope (Figure S3). Moreover, IL-10 has shown to induce expression of IL-4Rα, and M2 macrophages produce both IL-10 and IL-4, which may create a feed-forward process when IL-10 and IL-4 are overexpressed at the injured site.[12,21]

Immunomodulation by anti-inflammatory cytokines creates positive effects on axonal regrowth after SCI as a function of time. In the neuroinflammatory microenvironment, the M1 phenotype produces pro-inflammatory cytokines that are cytotoxic to neurons and cause them to extend short neurite sprouts after SCI.[10,32,33] Lentivirus-induced expression of IL-10 and IL-4 promoted both descending and ascending axonal tracts regrowth into the channels of the implanted bridge compared with empty bridges and vCtrl. IL-10 has been shown to upregulate anti-apoptotic factors such as B cell lymphoma 2 (Bcl-2) and to provide a direct trophic influence on neurons to overcome the neurotoxic microenvironment.[22,23,25] IL-4 controls macrophage activation in the acute SCI phase and reduces the release of pro-inflammatory factors at the injury.[24,25,38] In the experiments reported herein, IL-10 and IL-4 had a similar impact on inflammation-related gene expression dynamics, although a few differences in the dynamics were observed (e.g., *Retnla*). Moreover, the M2 phenotype forms in response to IL-10 and IL-4, and upregulates Arg1 activity, which in turn promotes overexpression of polyamines. Polyamines activate downstream of cAMP to enhance axonal regrowth against a myelin inhibitory environment.[12,32,41] In addition, M2 macrophages are thought to promote removal of apoptotic and necrotic cells via CD206 without toxic byproducts.[13,32] M2 macrophages also upregulate the expression level of *Retnla* (also known as Found in inflammatory zone1 [*Fizz1*]), which diminishes inflammatory responses and inhibits caspase-3- and caspase-8-mediated cellular apoptosis with involvement of the ERK pathway.[34,42] Through these pathways, M2 macrophages may facilitate phagocytosis and nerve tissue remodeling to promote axonal regeneration after SCI.

In addition to phagocytosis and axonal regeneration, anti-inflammatory cytokines may promote axonal remyelination over time. As a major component of the regenerative process, remyelination is mediated by multipotent oligodendrocyte progenitor cells (OPCs) after CNS injury. Previous studies demonstrate that skewing the M1:M2 ratio toward M2 activation is required for the differentiation of OPCs after SCI.[43,44] *In vitro* study shows that M2-conditioned media enhance oligodendrocyte differentiation.[43–46] Moreover, activin-A, an M2 derived-regenerative factor, directly binds to OPCs and contributes to M2-mediated oligodendrocyte differentiation in remyelinating lesions.[45,46] Therefore, a switch to M2 from M1 is an essential part of the regenerative process for enhancing differentiation of oligodendrocytes for remyelination.[43,44] In this study, IL-10 and IL-4 had similar effects on gene expression associated with neuronal development and functional regeneration, with a few differences in dynamics (e.g., *Lhx5, Hoxd10*, and *Negr1*). Collectively, vIL-10 and vIL-4 delivery decreased inflammation, which upregulated the population of M2 macrophages leading to an increase in the number of oligodendrocyte-derived myelinated axons at the injury as a function of time.

Ultimately, providing spatial organization for axonal regeneration using multichannel bridges with anti-inflammatory cytokines created synergistic effects on functional recovery after SCI. Previously, we have demonstrated that a naked PLG bridge altered the chemical balance and physical cues toward a more permissive environment.[9,18,19,21] In addition, the bridge porosity enables endogenous supportive cells such as Schwann cells and fibroblasts to infiltrate into the injured area, then release growth factors and deposit growth-stimulating extracellular matrix (ECM), leading to long-term axonal growth.[9,15,18,19] Furthermore, our gene expression data herein showed that the bridge itself upregulated axonal guidance- and synaptogenesis-associated gene expression compared with SCI only (Figures 2G and 6B).

While myelinated axons are observed in the middle of the bridge, Schwann cell-derived myelinated axons are observed particularly around and outside of the bridge and are significantly increased in both vIL-10 and vIL-4 relative to vCtrl. Both oligodendrocytes- and Schwann cell-derived remyelination of spared and regenerating axons have been shown to recover saltatory conduction and carry signals across the injury site, which are considered key factors for functional recovery.[47,48] We have shown that naked PLG bridges can support descending axonal regeneration and an increase in growth-associated protein (GAP)-43 above and below the implantation site, followed by the emergence of functional recovery on a forepaw cylinder reaching task.[16] Furthermore, previous studies demonstrate that spontaneous axonal sprouting after injury results in rewiring new synaptic connections and/or strengthening of existing synapses with other

Figure 5. Axonal Regrowth and Remyelination, and Source of Myelination in the Chronic Phase of SCI (Day 84)

(A and B) Immunofluorescence of myelinated axons from the implanted area delivering empty bridge, vCtrl, vIL-10, and vIL-4 at the rostral area (scale bar, 50 μm) (A). The line indicates the implanted bridge area for quantification, and dashed line is for higher magnification area in (B). White arrowheads indicate $NF200^+/MBP^+$ axons, and white arrows show $NF200^+/MBP^+/P0^+$ axons. (C) Quantification of total number of axons ($NF200^+$), unmyelinated axons ($NF200^+/MBP^-$), and myelinated axons ($NF200^+/MBP^+$) in each condition. (D) Percentage of axons that was myelinated within the bridge area. (E) Source of myelination in the chronic phase. Total quantification of oligodendrocyte-derived myelinated axons ($NF200^+/MBP^+/P0^-$) and Schwann cell-derived myelinated axons ($NF200^+/MBP^+/P0^+$) in all conditions. (F) Percentage of axons that was myelinated by oligodendrocytes. The statistical test was completed using a one- or two-way ANOVA with Tukey's post hoc test where $^*p < 0.05$, $^{**}p < 0.01$, and $^{\&}p < 0.0001$ compared with vCtrl group, and $^{\#}p < 0.05$, $^{\#\#}p < 0.01$, and $^{\&}p < 0.0001$ compared with bridge only group; mean ± SEM and n = 5/group.

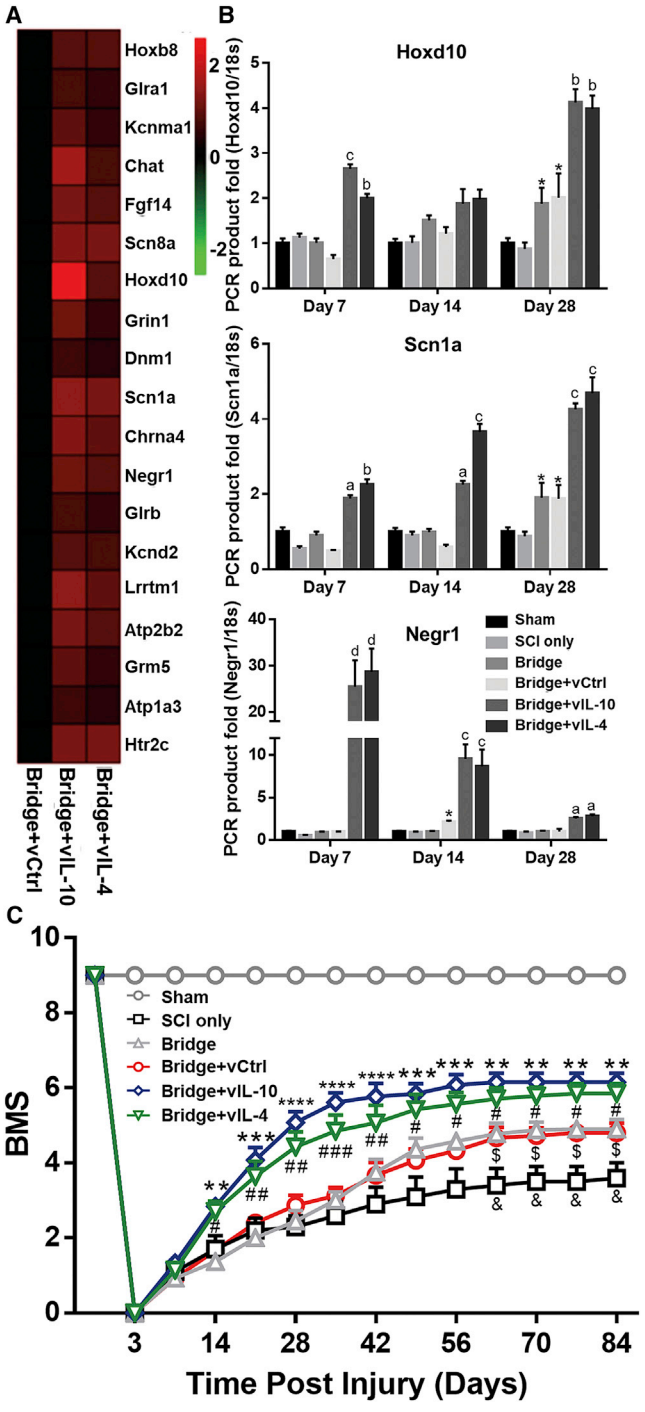

Figure 6. Locomotor Functional Recovery after SCI

(A) cDNA microarray heatmap shows that vIL-10 and vIL-4 upregulate locomotor recovery (GO:0007626)-associated gene expression relative to vCtrl. (B) Selected genes for cluster were validated via real-time qPCR over time. $^{a}p < 0.01$, $^{b}p < 0.01$, $^{c}p < 0.001$, and $^{d}p < 0.0001$ compared with vCtrl and $^{*}p < 0.05$ compared with SCI only (n = 5–6/group and time point, mean ± SEM, two-way ANOVA and Tukey post hoc test). (C) The ipsilateral hindlimb locomotor function was tested for the BMS weekly for 12 weeks after SCI. $^{**}p < 0.01$, $^{***}p < 0.001$, and $^{****}p < 0.0001$ Bridge+vIL-10 versus Bridge+vCtrl; $^{\#}p < 0.05$, $^{\#\#}p < 0.01$, and $^{\#\#\#}p < 0.001$ Bridge+vIL-4 versus Bridge+vCtrl; $^{\$}p < 0.05$ Bridge versus SCI only; and $^{\&}p < 0.05$ Bridge+vCtrl versus SCI only (n = 15/group, mean ± SEM, a two-way ANOVA with Dunnett's post hoc test).

spinal neurons, enhancing locomotor recovery in hemisection SCI.[49,50] Taken together, multichannel bridges with anti-inflammatory cytokines provide a permissive microenvironment for improved axonal sparing and regenerating resulting in greater locomotor recovery compared with control. Furthermore, locomotor recovery in the chronic phase may be associated with both improved axonal regeneration and sparing and remyelination at the injury site, which may result from synergistic effects of both immunomodulation by anti-inflammatory cytokines and topographical guidance via multichannel bridge over time. While most studies show improved functional recovery by anti-inflammatory factors, others have indicated that they may have negative effects on locomotor recovery after SCI.[51,52] This discrepancy may be because of differences in the rodent stains, SCI models, and/or delivery methods.

Localized delivery of therapeutics to the injured spinal cord has been unable to achieve long-term expression of therapeutics without additional surgery procedures. Although osmotic pumps and catheters have been extensively used for long-term sustained delivery of therapeutics, implantation inside the intrathecal space has been shown to generate scar tissue and additional damage at the implanted site.[53,54] Recently, as alternative methods to reduce tissue damage, therapeutics have been delivered intramuscularly or intravenously.[55,56] While these methods reduce the additional damage to spinal cord, they do not localize the therapies, and increased dosages can initiate an immune response.[55,57] A major challenge to cytokine therapy is their short half-life and instability in circulation, necessitating repeated administration.[21,58] Systemic overexpression of IL-10 and IL-4 has been the focus of previous reports by others who have not used a bridge. These reports have been conflicting, with some reports indicating neuroprotective effects with downregulated pro-inflammation and others indicating tissue damage with impaired locomotor functions.[52,58,59] These studies have largely focused on characterizing the immune response over short times. Herein, we identified that the expression of IL-10 and IL-4 promoted a more anti-inflammatory phenotype, yet also investigated the extent of regeneration out to 12 weeks, which indicated axon growth, myelination, and enhanced functional. In addition, we report that delivery of anti-inflammatory cytokine-encoding lentivirus from multichannel bridges provides a tool for long-term and sustained localized expression of potential therapeutics for tissue regeneration without additional damage. These observations are supported by a previous study that demonstrated that local lentiviral vector delivery of sonic hedgehog could lead to sustained and localized transgene expression over 12 weeks at the injured spinal cord site.[35] While the results herein demonstrate that anti-inflammatory cytokines effectively improve functional recovery, transgene expression requires a week to achieve significant levels. Therefore, earlier or alternative intervention may be required to restrict acute immune response-mediated tissue damage.

Nanoparticles (NPs) have received increasing attention in recent years as a tool for immune modulation in various diseases.[60,61] NPs can be utilized to target immune cells to attenuate their potential for causing immune pathology because they are generally considered as invasive pathogens and recognized rapidly by innate immune mechanisms.[60–62] Furthermore, NPs can be employed to deliver alone or in any combination,[62,63] thus delivery of NPs in combination with anti-inflammatory cytokines could act synergistically to promote further regeneration.

Collectively, the current study demonstrates that multichannel bridges and localized expression of anti-inflammatory cytokines can modulate the neuroinflammatory microenvironment after SCI. Localized IL-10 and IL-4 expression enhances macrophage polarization from a pro-inflammatory M1 to a pro-regenerative M2 phenotype compared with control. Under these conditions, the number of axons and oligodendrocyte-derived myelinated axons are significantly increased relative to control over time. Moreover, expression of anti-inflammatory cytokines promotes locomotor recovery after SCI. Our results suggest that providing a permissive environment for regeneration by a multichannel bridge, combined with localized anti-inflammatory cytokines gene delivery, may provide a novel therapeutic strategy to overcome a neuroinflammatory microenvironment for nerve regeneration after SCI.

MATERIALS AND METHODS

Virus Production

Lentivirus was produced from HEK293T cells based on established methods.[9,20] The objective in delivering the lentivirus was to promote expression of secreted IL-10 and IL-4 in the bridge. Thus, VSV-G pseudotyped virus with CMV promoter-driven cytokines was employed, which has been reported in previous studies delivering lentivirus from a multichannel bridge,[9,20,21] because this lentivirus can transduce multiple cell types and produce sustained transgene expression. Cells were co-transfected using third-generation lentiviral packaging vectors (pMDL-GagPol, pRSV-Rev, pIVS-VSV-G) and the gene of interest (pLenti-CMV-Luciferase or pLenti-CMV-Human IL10 or pLenti-CMV-Human IL4) using Lipofectamine 2000 (Life Technologies, Grand Island, NY, USA). After 48 hr, supernatant was collected and concentrated in PEG-it (System Biosciences, Mountain View, CA, USA) for 24 hr. Then, the supernatant was precipitated using ultracentrifugation, resuspended in PBS, and stored at −80°C until use. Virus titers were determined by a Lentivirus qPCR Titer Kit (Applied Biological Materials, Richmond, BC, Canada) and 2E9 IU/mL was used throughout the study.

Multichannel Bridges Fabrication

Multichannel bridges were fabricated using a gas foaming/particulate leaching method as previously described (Figure S1A).[9,15] In brief, PLG (75:25 lactide:glycolide; intravenous [i.v.] 0.76 dL/g; Lakeshore Biomaterials, Birmingham, AL, USA) was dissolved in dichloromethane (6% w/w) and emulsified in 1% poly(ethylene-alt-maleic anhydride) using a homogenizer (PolyTron 3100; Kinematica, Littau, Switzerland) to create microspheres (z-average diameter ~1 μm). D-sucrose (Sigma Aldrich), D-glucose (Sigma Aldrich), and dextran molecular weight (MW) 100,000 (Sigma Aldrich) were mixed at a ratio of 5.3:2.5:1, respectively, by mass. The mixture was caramelized, cooled, and drawn from solution using a Pasteur pipette to make a sugar fiber. These fibers were coated with a 1:1 mixture of PLG microspheres and salt, then pressed into a salt-lined aluminum mold. Next, the bridge was equilibrated, and gas formed with high-pressure CO_2 gas (800 psi) for 16 hr in a custom-made pressure vessel. The pressure was released over a period of 40 min, which fused adjacent microspheres to produce a continuous polymer structure. The bridges were cut into 2-mm sections, and the porogen was leached in water for 2 hr. The bridges were dried overnight and stored in a desiccator.

Virus Loading into the Multichannel Bridges

Bridges were disinfected in 70% of ethanol and washed with water, then dried at room temperature. In order to maximize lentivirus loading into bridges, we performed repeated addition of lentiviruses. Initially, 2 μL of virus was added onto the bridge, waiting for 2 min until it was completely adsorbed. We performed these procedures three additional times; then, bridges were stored at −80°C until use.

Spinal Cord Hemisection Injury Model and Animal Care

All animal surgery procedures and animal care were performed according to the Animal Care and Use Committee guideline at the University of Michigan. A mouse hemisection model of SCI was performed as described previously.[9,17] C57/BL6 female mice (6–8 weeks old; The Jackson Laboratory, Bar Harbor, ME, USA) were anesthetized using isoflurane (2%). A dorsal laminectomy was performed at T9–T10 level; then a 2-mm-long lateral of the midline spinal cord segment was removed to create a hemisection SCI mouse model. Bridges were implanted in the injury site and covered using Gelform (Pfizer, New York, NY, USA) (Figure S1B). Muscle was sutured together; then the skin was stapled. For postoperative animal care, Baytril (enrofloxacin 2.5 mg/kg subcutaneously [s.c.], once a day for 2 weeks), buprenorphine (0.1 mg/kg s.c., twice a day for 3 days), and lactate ringer solution (5 mL/100 g, once a day for 5 days) were administrated. Bladders were manually expressed twice a day until bladder reflexive function was observed.

ELISA

To measure the recombinant human IL-10 and IL-4 protein level from transfected host cells and tissues, we removed a 6-mm-long section of spinal cord, both rostral and caudal to the bridge, and homogenized it in radioimmunoprecipitation assay (RIPA) lysis and extraction buffer (Thermo Fisher Scientific, Waltham, MA, USA) with 10 μL of Halt Inhibitor Cocktail (Thermo Fisher Scientific) per milliliter of sample directly. Then, the homogenized tissue sample was incubated for 10 min at room temperature and centrifuged at 14,000 rpm for 30 min at 4°C to remove tissue debris. The protein concentration of each sample was estimated using Pierce BCA Protein Assay (Thermo Fisher Scientific); then samples were diluted accordingly. Human IL-10 and IL-4 concentration was subsequently assayed by Human IL-10 Quantikine ELISA Kit (R&D Systems, Minneapolis, MN, USA) and Human IL-4 ELISA Kit (LSbio, Seattle, WA, USA)

based on the manufacturer's instructions. Herein, we measured the human IL-10 and IL-4 protein levels to eliminate any confounding results with the expression of murine IL-10 and IL-4 protein by delivered lentiviral vectors. ELISA kits used for IL-10 and IL-4 quantification allow for distinguishing human IL-10 and IL-4 from murine IL-10 and IL-4, because the antibodies were not cross reactive as reported by the manufacturer.

RNA Isolation and cDNA Microarray

To isolate RNA, we removed the spinal cord tissues from all conditions (n = 5–6/group and time point; at days 3, 7, 14, and 28 post-SCI) and cut them into 6-mm segments centered on 2 mm of bridge region; samples were not pooled. We performed RNA isolation based on a previous study.[7] In brief, the spinal cord samples were homogenized using 1 mL of TRIzol reagent (Invitrogen, Carlsbad, CA, USA) with a tissue grinder. RNA isolation was followed by chloroform extraction and isopropanol precipitation. The extracted RNA was dissolved in 30 μL of RNase-free distilled water; then we measured RNA concentration using a NanoDrop 2000C (Thermo Scientific, Newark, DE, USA) with A260/A280 ratios between 1.9 and 2.1 for all samples. Total isolated RNA was stored at −80°C until use. For the cDNA microarray, gene expression analysis from each condition was conducted using the Mouse Gene ST 2.1 microarray platform (Affymetrix). Data were processed using the oligo R package. Raw output from the multi-array was converted to expression values through robust microarray averaging.[64] Data quality was assessed by principle component analysis. Sample in each group was normalized to expression values from a bridge+control virus group and log transformed. Probe set annotation was downloaded from BioConductor. GO accession number (Table S1) and analysis were performed using PANTHER.[65]

qRT-PCR

For the gene expression analysis, we performed qRT-PCR. cDNA was synthesized using an iScript cDNA Synthesis kit (Bio-Rad, Hercules, CA, USA) according to the manufacturer's guidelines. One microgram of RNA was used from each sample to synthesize cDNA. Primers were designed for real-time qPCR based on the previous study (Table S2).[6,32,66,67] 18 s-rRNA was used as an internal control. The real-time qPCR products were measured using the accumulation level of iQ SYBR Green Supermix (Bio-Rad) fluorescence following a manufacturer's protocol on CFX Connect Real-Time PCR Detection System (Bio-Rad). The gene expression level was normalized by the expression of 18 s-rRNA, and differences in gene expression were presented as fold ratios from sham spinal cord samples. Relative quantification was calculated as $X = 2^{-\Delta\Delta Ct}$, where $\Delta\Delta C_t = \Delta E - \Delta C_t$ and $\Delta E = C_{t,exp} - C_{t,18\ s\text{-}rRNA}$, $\Delta C_t = C_{t,\ sham} - C_{t,18\ s\text{-}rRNA}$.[68]

Immunofluorescence

Spinal cords containing multichannel bridge were collected at 14, 28, and 84 days after SCI and were snap frozen in isopentane and embedded in Tissue Tek O.C.T. compound (Sakura Finetek, Torrance, CA, USA) with 30% sucrose. Spinal cords were cryosectioned at 18 μm thickness in the transverse plane. The following antibodies were used for immunofluorescence: NF200 (1:200; Sigma-Aldrich), MBP (1:500, Santa Cruz Biotech, Dallas, TX, USA), P-zero myelin protein (P0) (1:250; Aves Labs, Tigard, OR, USA), F4/80 (1:200; AbD Serotec, Raleigh, NC, USA), Arg1 (1:100, clone N20; Santa Cruz Biotech), and Hoechst 33258 for counterstain (1:2,000, H3569; Fisher). Species-specific secondary antibodies were used for the detection (1:1,000; Fisher Scientific, unless otherwise noted); Alexa Fluor 555 goat anti-rabbit IgG (A-21429), Alexa Fluor 555 goat anti-mouse IgG (A-21424), Alexa Fluor 488 donkey anti-goat IgG (A-11055), Alexa Fluor 555 donkey anti-goat IgG (A-21432), Alexa Fluor 647 donkey anti-goat IgG (A-21447), Alexa Fluor 647 donkey anti-mouse IgG (A-31571). Nine spinal cord tissues were selected randomly from each rostral, middle, and caudal location of the implanted bridge from each animal of each condition (total of 27 tissues were investigated per animal). From the rostral edge of the bridge/tissue interface, analysis for rostral location was done at 300 μm, middle at 900 μm, and caudal at 1600 μm (Figure S1C). Tissues were imaged on an Axio Observer Z1 (Zeiss, Oberkochen, Germany) using a 10× or 20×/0.45 M27 apochromatic objective and an ORCA-Flash 4.0 V2 Digital CMOS camera (C11440-22CU; Hamamatsu Photonics, Hamamatsu City, Shizuoka, Japan). The number of immune-positive cells and axons within the implant bridge area were manually counted by blinded researchers independently. Multiple markers by co-staining were examined by evaluating pixel overlap of different channels in NIH ImageJ (Bethesda, MD, USA). The total number of macrophages and M2 phenotype macrophages were evaluated by determining $F4/80^+$ cells and $F4/80^+$/$arginase^+$ cells. Macrophages were identified by localizing $Hoechst^+$ staining to $F4/80^+$ immunoreactive cells and labeling them in ImageJ. Then the cell numbers were normalized to the counted area in each tissue section. To investigate the numbers of regenerated and myelinated neurofilaments, we used $NF200^+$, $NF200^+/MBP^+$, and $NF200^+/MBP^+/P0^+$ to identify the numbers of axons, myelinated axons, and myelinated axons by infiltrating Schwann cells, respectively. The percentage of myelinated axons was determined from the ratio of the number of myelinated axons ($NF200^+/MBP^+$) divided by the number of axons ($NF200^+$) within the bridge area. To determine the source of the myelination, we performed triple staining of NF200, MBP, and P0. $NF200^+/MBP^+/P0^-$ neurofilaments were considered as oligodendrocyte-derived myelination and $NF200^+/MBP^+/P0^+$ neurofilaments were myelinated neurofilaments by infiltrated Schwann cells. The fraction of oligodendrocyte-derived myelination was calculated as $NF200^+/MBP^+/P0^-$ neurofilaments divided by $NF200^+/MBP^+$ neurofilaments

Behavioral Test for Locomotor Function

Motor recovery in the ipsilateral hindlimb was accessed using open-field Basso Mouse Scale (BMS) locomotor rating scale after SCI.[29] The score is based on the hindlimb locomotor ability of SCI mice. SCI mice (n = 15/group) were observed in an open field for 4 min after they had gently adapted to the field. Only the ipsilateral hindlimb side was assessed at days 3 and then weekly after SCI for 12 weeks. The score was obtained by taking an average value of results from each experimental group. A baseline was determined prior to SCI.

In order to measure more detailed fine components of locomotor functions such as plantar stepping, coordination, paw position, normal posture, and tail stability, all SCI mice were also scored weekly using the BMS subscoring system from days 63 to 84 after SCI.[29] Animals were randomly assigned to treatment group, and assessment was performed by researchers blinded to the group.

Statistical Analysis

Unless noted otherwise, a one- or two-way ANOVA was used for multiple comparisons. For the statistical significance between groups, we performed Tukey's or Dunnett's post hoc testing or Šidák correction for the multiple comparisons. Pearson's correlation coefficient was used for determining the statistical significance of regression data. Type II errors were controlled at 0.2 level for all of the statistical tests to achieve reasonable statistical power analyses. Equal variance (ANOVA model) was validated and assumed for each study. Given the above parameters, appropriate sample size for each study and all statistical analyses were performed using G* Power Software,[69] OriginPro (OriginLab Corporation, Northampton, MA, USA), and Prism 6 (GraphPad Software, La Jolla, CA, USA). $p < 0.05$ was considered statistically significant, and all values were expressed in mean ± SEM.

SUPPLEMENTAL INFORMATION

Supplemental Information includes six figures and two tables and can be found with this article online at https://doi.org/10.1016/j.ymthe.2018.04.022.

AUTHOR CONTRIBUTIONS

Conceptualization and design of the study, J.P. and L.D.S.; Methodology, J.P., J.T.D., D.J.M., and L.D.S.; Investigation, J.P., J.T.D., D.J.M., and D.R.S.; Draft writing and review, J.P., J.T.D., D.R.S., B.J.C., A.J.A., and L.D.S.; Funding, B.J.C., A.J.A., and L.D.S.; Supervision, L.D.S.

ACKNOWLEDGMENTS

We thank the Unit for Laboratory Animal Medicine (ULAM) at the University of Michigan for animal care and maintenance and University of Michigan Microarray Core for microarray performance. This study was supported by the NIH (R01EB005678).

REFERENCES

1. Park, J., Lim, E., Back, S., Na, H., Park, Y., and Sun, K. (2010). Nerve regeneration following spinal cord injury using matrix metalloproteinase-sensitive, hyaluronic acid-based biomimetic hydrogel scaffold containing brain-derived neurotrophic factor. J. Biomed. Mater. Res. A *93*, 1091–1099.
2. Blesch, A., and Tuszynski, M.H. (2009). Spinal cord injury: plasticity, regeneration and the challenge of translational drug development. Trends Neurosci. *32*, 41–47.
3. Chen, Z., Park, J., Butler, B., Acosta, G., Vega-Alvarez, S., Zheng, L., Tang, J., McCain, R., Zhang, W., Ouyang, Z., et al. (2016). Mitigation of sensory and motor deficits by acrolein scavenger phenelzine in a rat model of spinal cord contusive injury. J. Neurochem. *138*, 328–338.
4. Yiu, G., and He, Z. (2006). Glial inhibition of CNS axon regeneration. Nat. Rev. Neurosci. *7*, 617–627.
5. David, S., López-Vales, R., and Wee Yong, V. (2012). Harmful and beneficial effects of inflammation after spinal cord injury: potential therapeutic implications. Handb. Clin. Neurol. *109*, 485–502.
6. Park, J., Zheng, L., Acosta, G., Vega-Alvarez, S., Chen, Z., Muratori, B., Cao, P., and Shi, R. (2015). Acrolein contributes to TRPA1 up-regulation in peripheral and central sensory hypersensitivity following spinal cord injury. J. Neurochem. *135*, 987–997.
7. Due, M.R., Park, J., Zheng, L., Walls, M., Allette, Y.M., White, F.A., and Shi, R. (2014). Acrolein involvement in sensory and behavioral hypersensitivity following spinal cord injury in the rat. J. Neurochem. *128*, 776–786.
8. Donnelly, D.J., and Popovich, P.G. (2008). Inflammation and its role in neuroprotection, axonal regeneration and functional recovery after spinal cord injury. Exp. Neurol. *209*, 378–388.
9. Tuinstra, H.M., Aviles, M.O., Shin, S., Holland, S.J., Zelivyanskaya, M.L., Fast, A.G., Ko, S.Y., Margul, D.J., Bartels, A.K., Boehler, R.M., et al. (2012). Multifunctional, multichannel bridges that deliver neurotrophin encoding lentivirus for regeneration following spinal cord injury. Biomaterials *33*, 1618–1626.
10. David, S., and Kroner, A. (2011). Repertoire of microglial and macrophage responses after spinal cord injury. Nat. Rev. Neurosci. *12*, 388–399.
11. Martinez, F.O., and Gordon, S. (2014). The M1 and M2 paradigm of macrophage activation: time for reassessment. F1000Prime Rep. *6*, 13.
12. Mantovani, A., Biswas, S.K., Galdiero, M.R., Sica, A., and Locati, M. (2013). Macrophage plasticity and polarization in tissue repair and remodelling. J. Pathol. *229*, 176–185.
13. Gordon, S. (2003). Alternative activation of macrophages. Nat. Rev. Immunol. *3*, 23–35.
14. Schmidt, C.E., and Leach, J.B. (2003). Neural tissue engineering: strategies for repair and regeneration. Annu. Rev. Biomed. Eng. *5*, 293–347.
15. De Laporte, L., Yang, Y., Zelivyanskaya, M.L., Cummings, B.J., Anderson, A.J., and Shea, L.D. (2009). Plasmid releasing multiple channel bridges for transgene expression after spinal cord injury. Mol. Ther. *17*, 318–326.
16. Pawar, K., Cummings, B.J., Thomas, A., Shea, L.D., Levine, A., Pfaff, S., and Anderson, A.J. (2015). Biomaterial bridges enable regeneration and re-entry of corticospinal tract axons into the caudal spinal cord after SCI: association with recovery of forelimb function. Biomaterials *65*, 1–12.
17. Tuinstra, H.M., Margul, D.J., Goodman, A.G., Boehler, R.M., Holland, S.J., Zelivyanskaya, M.L., Cummings, B.J., Anderson, A.J., and Shea, L.D. (2014). Long-term characterization of axon regeneration and matrix changes using multiple channel bridges for spinal cord regeneration. Tissue Eng. Part A *20*, 1027–1037.
18. Thomas, A.M., Kubilius, M.B., Holland, S.J., Seidlits, S.K., Boehler, R.M., Anderson, A.J., Cummings, B.J., and Shea, L.D. (2013). Channel density and porosity of degradable bridging scaffolds on axon growth after spinal injury. Biomaterials *34*, 2213–2220.
19. Yang, Y., De Laporte, L., Zelivyanskaya, M.L., Whittlesey, K.J., Anderson, A.J., Cummings, B.J., and Shea, L.D. (2009). Multiple channel bridges for spinal cord injury: cellular characterization of host response. Tissue Eng. Part A *15*, 3283–3295.
20. Thomas, A.M., Seidlits, S.K., Goodman, A.G., Kukushliev, T.V., Hassani, D.M., Cummings, B.J., Anderson, A.J., and Shea, L.D. (2014). Sonic hedgehog and neurotrophin-3 increase oligodendrocyte numbers and myelination after spinal cord injury. Integr. Biol. *6*, 694–705.
21. Margul, D.J., Park, J., Boehler, R.M., Smith, D.R., Johnson, M.A., McCreedy, D.A., He, T., Ataliwala, A., Kukushliev, T.V., Liang, J., et al. (2016). Reducing neuroinflammation by delivery of IL-10 encoding lentivirus from multiple-channel bridges. Bioeng. Transl. Med. *1*, 136–148.
22. Thompson, C.D., Zurko, J.C., Hanna, B.F., Hellenbrand, D.J., and Hanna, A. (2013). The therapeutic role of interleukin-10 after spinal cord injury. J. Neurotrauma *30*, 1311–1324.
23. Zhou, Z., Peng, X., Insolera, R., Fink, D.J., and Mata, M. (2009). Interleukin-10 provides direct trophic support to neurons. J. Neurochem. *110*, 1617–1627.
24. Bhattacharjee, A., Shukla, M., Yakubenko, V.P., Mulya, A., Kundu, S., and Cathcart, M.K. (2013). IL-4 and IL-13 employ discrete signaling pathways for target gene expression in alternatively activated monocytes/macrophages. Free Radic. Biol. Med. *54*, 1–16.
25. Garcia, E., Aguilar-Cevallos, J., Silva-Garcia, R., and Ibarra, A. (2016). Cytokine and growth factor activation in vivo and in vitro after spinal cord injury. Mediators Inflamm. *2016*, 9476020.

26. Pfaff, S.L., Mendelsohn, M., Stewart, C.L., Edlund, T., and Jessell, T.M. (1996). Requirement for LIM homeobox gene Isl1 in motor neuron generation reveals a motor neuron-dependent step in interneuron differentiation. Cell *84*, 309–320.

27. Oohashi, T., Edamatsu, M., Bekku, Y., and Carulli, D. (2015). The hyaluronan and proteoglycan link proteins: organizers of the brain extracellular matrix and key molecules for neuronal function and plasticity. Exp. Neurol. *274* (Pt B), 134–144.

28. Shin, H.Y., Hong, Y.H., Jang, S.S., Chae, H.G., Paek, S.L., Moon, H.E., Kim, D.G., Kim, J., Paek, S.H., and Kim, S.J. (2010). A role of canonical transient receptor potential 5 channel in neuronal differentiation from A2B5 neural progenitor cells. PLoS ONE *5*, e10359.

29. Basso, D.M., Fisher, L.C., Anderson, A.J., Jakeman, L.B., McTigue, D.M., and Popovich, P.G. (2006). Basso Mouse Scale for locomotion detects differences in recovery after spinal cord injury in five common mouse strains. J. Neurotrauma *23*, 635–659.

30. Hill, R.L., Zhang, Y.P., Burke, D.A., Devries, W.H., Zhang, Y., Magnuson, D.S., Whittemore, S.R., and Shields, C.B. (2009). Anatomical and functional outcomes following a precise, graded, dorsal laceration spinal cord injury in C57BL/6 mice. J. Neurotrauma *26*, 1–15.

31. Ji, B., Case, L.C., Liu, K., Shao, Z., Lee, X., Yang, Z., Wang, J., Tian, T., Shulga-Morskaya, S., Scott, M., et al. (2008). Assessment of functional recovery and axonal sprouting in oligodendrocyte-myelin glycoprotein (OMgp) null mice after spinal cord injury. Mol. Cell. Neurosci. *39*, 258–267.

32. Kigerl, K.A., Gensel, J.C., Ankeny, D.P., Alexander, J.K., Donnelly, D.J., and Popovich, P.G. (2009). Identification of two distinct macrophage subsets with divergent effects causing either neurotoxicity or regeneration in the injured mouse spinal cord. J. Neurosci. *29*, 13435–13444.

33. Gensel, J.C., and Zhang, B. (2015). Macrophage activation and its role in repair and pathology after spinal cord injury. Brain Res. *1619*, 1–11.

34. Chung, M.J., Liu, T., Ullenbruch, M., and Phan, S.H. (2007). Antiapoptotic effect of found in inflammatory zone (FIZZ)1 on mouse lung fibroblasts. J. Pathol. *212*, 180–187.

35. Thomas, A.M., Palma, J.L., and Shea, L.D. (2015). Sponge-mediated lentivirus delivery to acute and chronic spinal cord injuries. J. Control. Release *204*, 1–10.

36. Hanada, T., and Yoshimura, A. (2002). Regulation of cytokine signaling and inflammation. Cytokine Growth Factor Rev. *13*, 413–421.

37. Schottelius, A.J.G., Mayo, M.W., Sartor, R.B., and Baldwin, A.S., Jr. (1999). Interleukin-10 signaling blocks inhibitor of kappaB kinase activity and nuclear factor kappaB DNA binding. J. Biol. Chem. *274*, 31868–31874.

38. Wirjatijasa, F., Dehghani, F., Blaheta, R.A., Korf, H.W., and Hailer, N.P. (2002). Interleukin-4, interleukin-10, and interleukin-1-receptor antagonist but not transforming growth factor-beta induce ramification and reduce adhesion molecule expression of rat microglial cells. J. Neurosci. Res. *68*, 579–587.

39. Gadani, S.P., Cronk, J.C., Norris, G.T., and Kipnis, J. (2012). IL-4 in the brain: a cytokine to remember. J. Immunol. *189*, 4213–4219.

40. Vidal, P.M., Lemmens, E., Dooley, D., and Hendrix, S. (2013). The role of "anti-inflammatory" cytokines in axon regeneration. Cytokine Growth Factor Rev. *24*, 1–12.

41. Cai, D., Deng, K., Mellado, W., Lee, J., Ratan, R.R., and Filbin, M.T. (2002). Arginase I and polyamines act downstream from cyclic AMP in overcoming inhibition of axonal growth MAG and myelin in vitro. Neuron *35*, 711–719.

42. Pesce, J.T., Ramalingam, T.R., Wilson, M.S., Mentink-Kane, M.M., Thompson, R.W., Cheever, A.W., Urban, J.F., Jr., and Wynn, T.A. (2009). Retnla (relmalpha/fizz1) suppresses helminth-induced Th2-type immunity. PLoS Pathog. *5*, e1000393.

43. Miron, V.E., Boyd, A., Zhao, J.W., Yuen, T.J., Ruckh, J.M., Shadrach, J.L., van Wijngaarden, P., Wagers, A.J., Williams, A., Franklin, R.J.M., and Ffrench-Constant, C. (2013). M2 microglia and macrophages drive oligodendrocyte differentiation during CNS remyelination. Nat. Neurosci. *16*, 1211–1218.

44. Miron, V.E., and Franklin, R.J. (2014). Macrophages and CNS remyelination. J. Neurochem. *130*, 165–171.

45. He, J.T., Mang, J., Mei, C.L., Yang, L., Wang, J.Q., Xing, Y., Yang, H., and Xu, Z.X. (2011). Neuroprotective effects of exogenous activin A on oxygen-glucose deprivation in PC12 cells. Molecules *17*, 315–327.

46. de Kretser, D.M., O'Hehir, R.E., Hardy, C.L., and Hedger, M.P. (2012). The roles of activin A and its binding protein, follistatin, in inflammation and tissue repair. Mol. Cell. Endocrinol. *359*, 101–106.

47. Zawadzka, M., Rivers, L.E., Fancy, S.P.J., Zhao, C., Tripathi, R., Jamen, F., Young, K., Goncharevich, A., Pohl, H., Rizzi, M., et al. (2010). CNS-resident glial progenitor/stem cells produce Schwann cells as well as oligodendrocytes during repair of CNS demyelination. Cell Stem Cell *6*, 578–590.

48. Franklin, R.J., and Ffrench-Constant, C. (2008). Remyelination in the CNS: from biology to therapy. Nat. Rev. Neurosci. *9*, 839–855.

49. Schnell, L., and Schwab, M.E. (1993). Sprouting and regeneration of lesioned corticospinal tract fibres in the adult rat spinal cord. Eur. J. Neurosci. *5*, 1156–1171.

50. Helgren, M.E., and Goldberger, M.E. (1993). The recovery of postural reflexes and locomotion following low thoracic hemisection in adult cats involves compensation by undamaged primary afferent pathways. Exp. Neurol. *123*, 17–34.

51. Bethea, J.R., Nagashima, H., Acosta, M.C., Briceno, C., Gomez, F., Marcillo, A.E., Loor, K., Green, J., and Dietrich, W.D. (1999). Systemically administered interleukin-10 reduces tumor necrosis factor-alpha production and significantly improves functional recovery following traumatic spinal cord injury in rats. J. Neurotrauma *16*, 851–863.

52. Takami, T., Oudega, M., Bethea, J.R., Wood, P.M., Kleitman, N., and Bunge, M.B. (2002). Methylprednisolone and interleukin-10 reduce gray matter damage in the contused Fischer rat thoracic spinal cord but do not improve functional outcome. J. Neurotrauma *19*, 653–666.

53. Jones, L.L., and Tuszynski, M.H. (2001). Chronic intrathecal infusions after spinal cord injury cause scarring and compression. Microsc. Res. Tech. *54*, 317–324.

54. Ziemba, A.M., and Gilbert, R.J. (2017). Biomaterials for local, controlled drug delivery to the injured spinal cord. Front. Pharmacol. *8*, 245.

55. Foust, K.D., Nurre, E., Montgomery, C.L., Hernandez, A., Chan, C.M., and Kaspar, B.K. (2009). Intravascular AAV9 preferentially targets neonatal neurons and adult astrocytes. Nat. Biotechnol. *27*, 59–65.

56. Paul, C., Samdani, A.F., Betz, R.R., Fischer, I., and Neuhuber, B. (2009). Grafting of human bone marrow stromal cells into spinal cord injury: a comparison of delivery methods. Spine *34*, 328–334.

57. Snyder, B.R., Gray, S.J., Quach, E.T., Huang, J.W., Leung, C.H., Samulski, R.J., Boulis, N.M., and Federici, T. (2011). Comparison of adeno-associated viral vector serotypes for spinal cord and motor neuron gene delivery. Hum. Gene Ther. *22*, 1129–1135.

58. Lima, R., Monteiro, S., Lopes, J.P., Barradas, P., Vasconcelos, N.L., Gomes, E.D., Assunção-Silva, R.C., Teixeira, F.G., Morais, M., Sousa, N., et al. (2017). Systemic interleukin-4 administration after spinal cord injury modulates inflammation and promotes neuroprotection. Pharmaceuticals (Basel) *10*, E83.

59. Pearse, D.D., Marcillo, A.E., Oudega, M., Lynch, M.P., Wood, P.M., and Bunge, M.B. (2004). Transplantation of Schwann cells and olfactory ensheathing glia after spinal cord injury: does pretreatment with methylprednisolone and interleukin-10 enhance recovery? J. Neurotrauma *21*, 1223–1239.

60. Getts, D.R., Shea, L.D., Miller, S.D., and King, N.J. (2015). Harnessing nanoparticles for immune modulation. Trends Immunol. *36*, 419–427.

61. Kim, E.S., Ahn, E.H., Dvir, T., and Kim, D.H. (2014). Emerging nanotechnology approaches in tissue engineering and regenerative medicine. Int. J. Nanomedicine *9* (*Suppl 1*), 1–5.

62. McCarthy, D.P., Hunter, Z.N., Chackerian, B., Shea, L.D., and Miller, S.D. (2014). Targeted immunomodulation using antigen-conjugated nanoparticles. Wiley Interdiscip. Rev. Nanomed. Nanobiotechnol. *6*, 298–315.

63. Heo, M.B., and Lim, Y.T. (2014). Programmed nanoparticles for combined immunomodulation, antigen presentation and tracking of immunotherapeutic cells. Biomaterials *35*, 590–600.

64. Bolstad, B.M., Irizarry, R.A., Astrand, M., and Speed, T.P. (2003). A comparison of normalization methods for high density oligonucleotide array data based on variance and bias. Bioinformatics *19*, 185–193.

65. Mi, H., Huang, X., Muruganujan, A., Tang, H., Mills, C., Kang, D., and Thomas, P.D. (2017). PANTHER version 11: expanded annotation data from Gene Ontology and Reactome pathways, and data analysis tool enhancements. Nucleic Acids Res. *45* (D1), D183–D189.

66. Roszer, T. (2015). Understanding the mysterious M2 macrophage through activation markers and effector mechanisms. Mediat. Inflamm. *2015*, 816460.

67. Jablonski, K.A., Amici, S.A., Webb, L.M., Ruiz-Rosado, Jde.D., Popovich, P.G., Partida-Sanchez, S., and Guerau-de-Arellano, M. (2015). Novel markers to delineate murine M1 and M2 macrophages. PLoS ONE *10*, e0145342.

68. Livak, K.J., and Schmittgen, T.D. (2001). Analysis of relative gene expression data using real-time quantitative PCR and the 2(-Delta Delta C(T)) method. Methods *25*, 402–408.

69. Faul, F., Erdfelder, E., Lang, A.G., and Buchner, A. (2007). G*Power 3: a flexible statistical power analysis program for the social, behavioral, and biomedical sciences. Behav. Res. Methods *39*, 175–191.

YMTHE, Volume *26*

Supplemental Information

Local Immunomodulation with Anti-inflammatory Cytokine-Encoding Lentivirus Enhances Functional Recovery after Spinal Cord Injury

Jonghyuck Park, Joseph T. Decker, Daniel J. Margul, Dominique R. Smith, Brian J. Cummings, Aileen J. Anderson, and Lonnie D. Shea

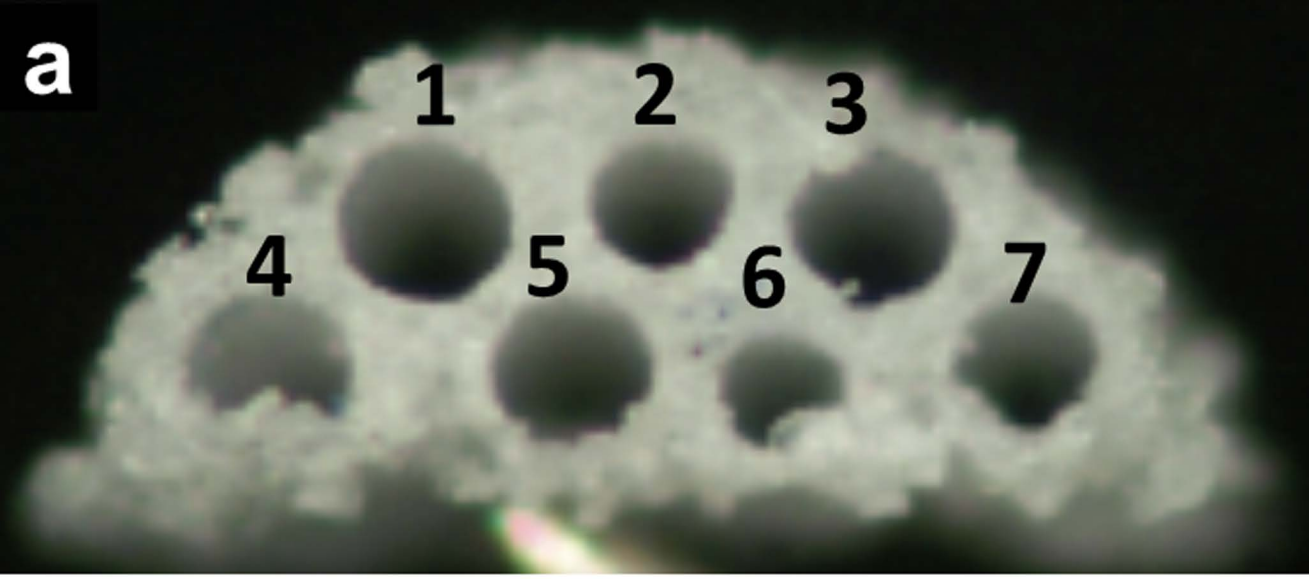
a
1
2
3
4
5
6
7

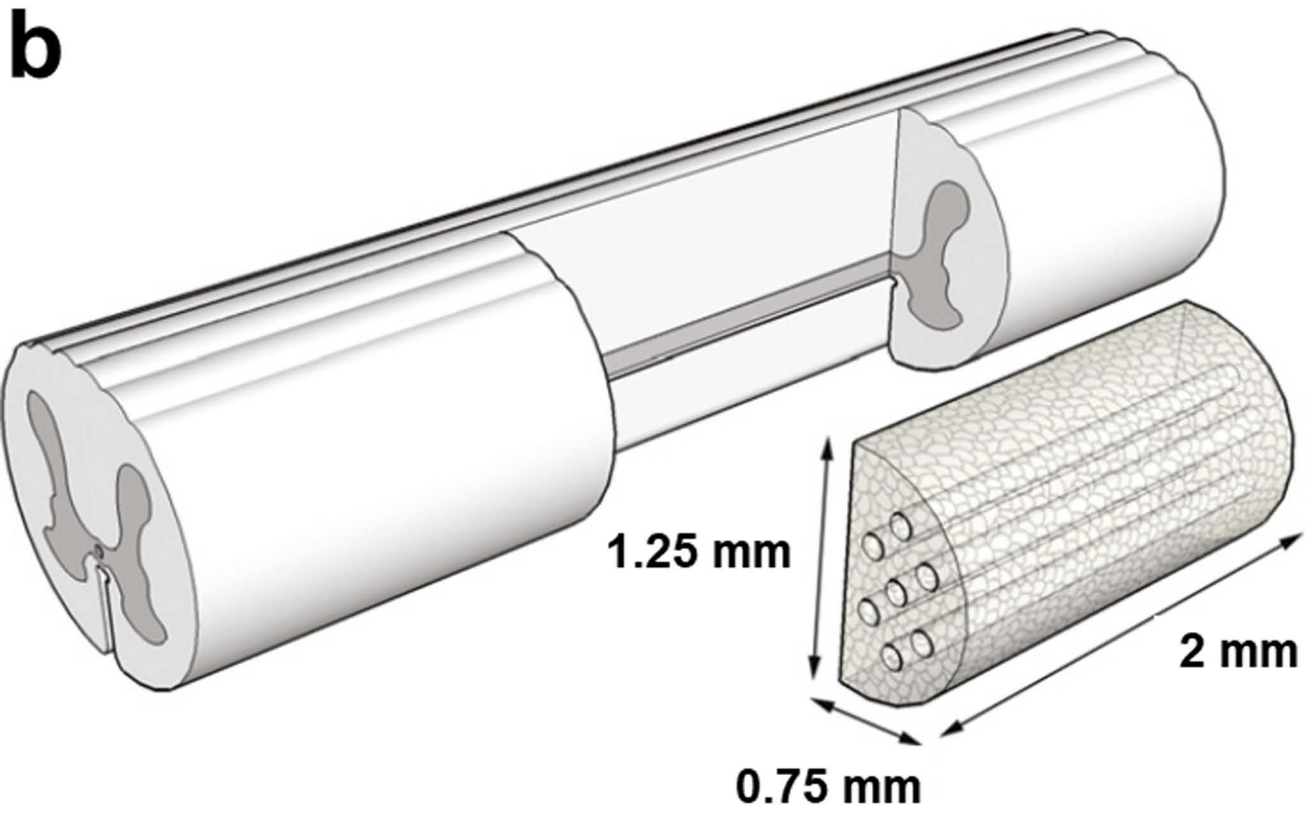
b
1.25 mm
2 mm
0.75 mm

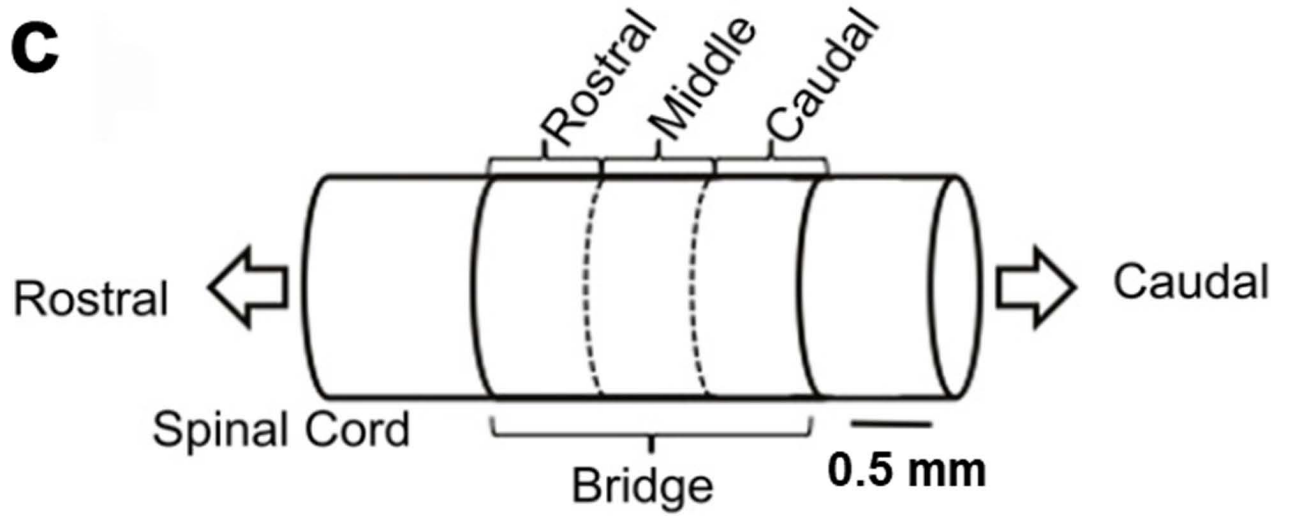
c
Rostral
Middle
Caudal
Rostral
Caudal
Spinal Cord
Bridge
0.5 mm

a
Cd28
Slc11a1
Fcgr4
Cd48
Cxcr4
Itgb2
Stat6
Havcr2
Milr1
Cd300a
Dock2
Zfp36l1
Syk
Cd180
Lcp1
Lgals1
Il7r
Myo1f
Vav1
Nfatc1
Dock8
Anxa1
Blnk
Lbp
Cdk6
Cxcl5
Anxa3
Tec
Lat2
Pilrb1
Cxcl12
Bridge + vCtrl
Bridge + vIL-10
Bridge + vI-L4
b
Ly96
Slc11a1
Fn1
Mapkapk2
Itgb2
Havcr2
Aoc3
Cd300a
Ccl9
Ccl6
Ccl3
Syk
Cd180
Stab1
Cd14
Lipa
Il1rn
Thbs1
Lbp
Il1b
Cd5l
Ecm1
Ptafr
Tnfrsf1b
Cxcl5
C3ar1
Tgfb1
Il4ra
C5ar1
Mrgpra3
Nupr1
Adam8
Cyba
Casp4
Ccr1
Tlr13
Cybb
Tlr8
Tlr7
Bridge + vCtrl
Bridge + vIL-10
Bridge + vI-L4
c
Thbs1
Lbp
Il1b
Ecm1
Ptafr
Cxcl5
Cxcl12
C3ar1
Tgfb1
C5ar1
Adam8
Ccr1
d
Ly96
Cd28
Slc11a1
Cd84
Ikbke
Slamf7
Stat6
Havcr2
Milr1
Cd300a
Dock2
Bcl6b
Ccl9
Ccl6
Ccl3
Syk
Cd180
Bridge + vCtrl
Bridge + vIL-10
Bridge + vIL-4
e
Gabrb2
Cntnap1
Nptx1
Spock1
Kcnma1
Chat
Slitrk1
Hoxc10
Faim2
Htr7
Hoxd10
Slc12a5
Grin1
Stxbp1
Chn1
Lingo4
Olfm3
Efna3
Cnr1
Sh3gl2
Lhx5
Cntnap2
Cntn6
Cntn4
Atp2b2
Bridge + vCtrl
Bridge + vIL-10
Bridge + vIL-4
f
Syt2
Rims1
Syn3
Gabrb2
Gabrg2
Glra1
Nrxn3
Cadps
Kcnma1
Chat
Fgf14
Syt10
Slc5a7
Pcdhb3
Htr7
Syt13
Slc12a5
Oprl1
Grin1
Dnm1
Stxbp1
Napb
Chrna4
Glrb
Gabrg1
Bridge + vCtrl
Bridge + vIL-10
Bridge + vIL-4
2
0
-2

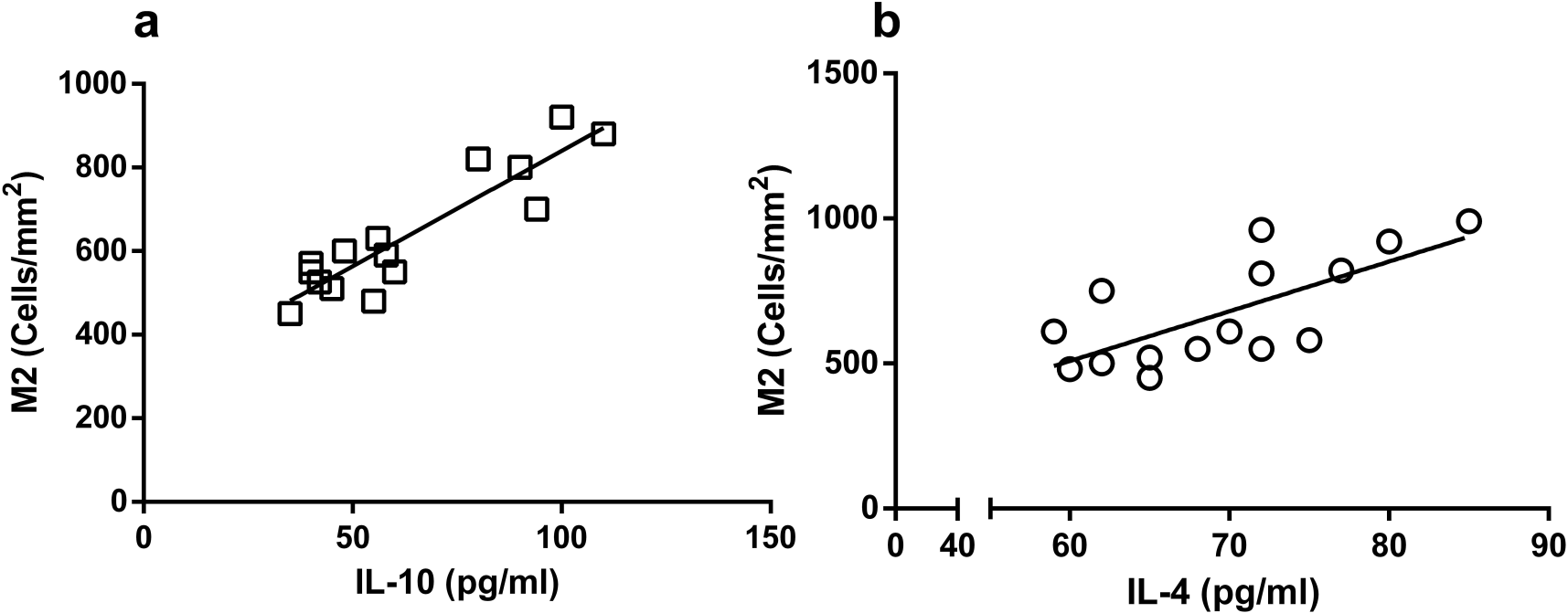
a
1000
800
600
400
200
0
M2 (Cells/mm2)
0
50
100
150
IL-10 (pg/ml)
b
1500
1000
500
0
M2 (Cells/mm2)
0
40
60
70
80
90
IL-4 (pg/ml)

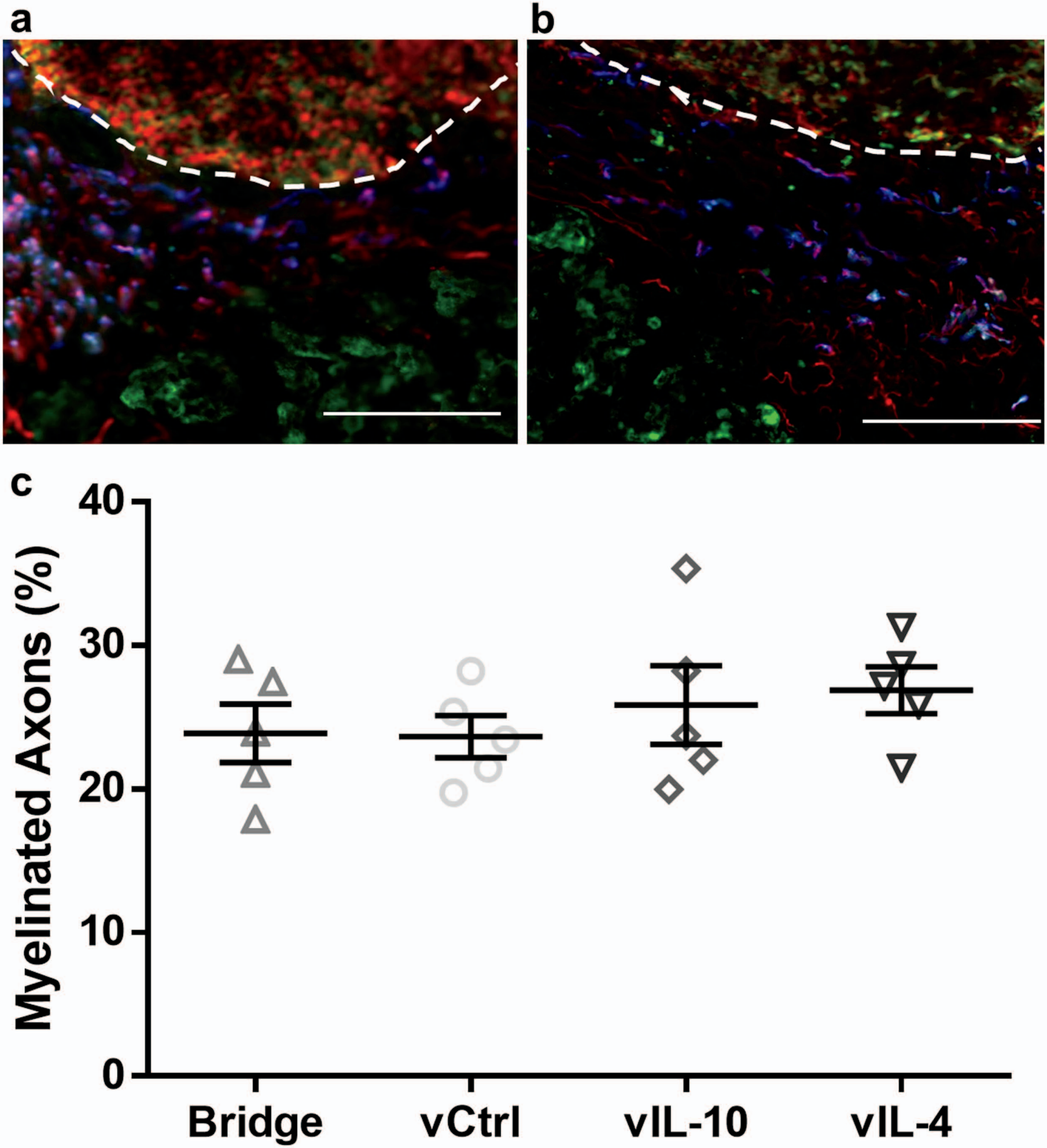
a
b
c
Myelinated Axons (%)
40
30
20
10
0
Bridge
vCtrl
vIL-10
vIL-4

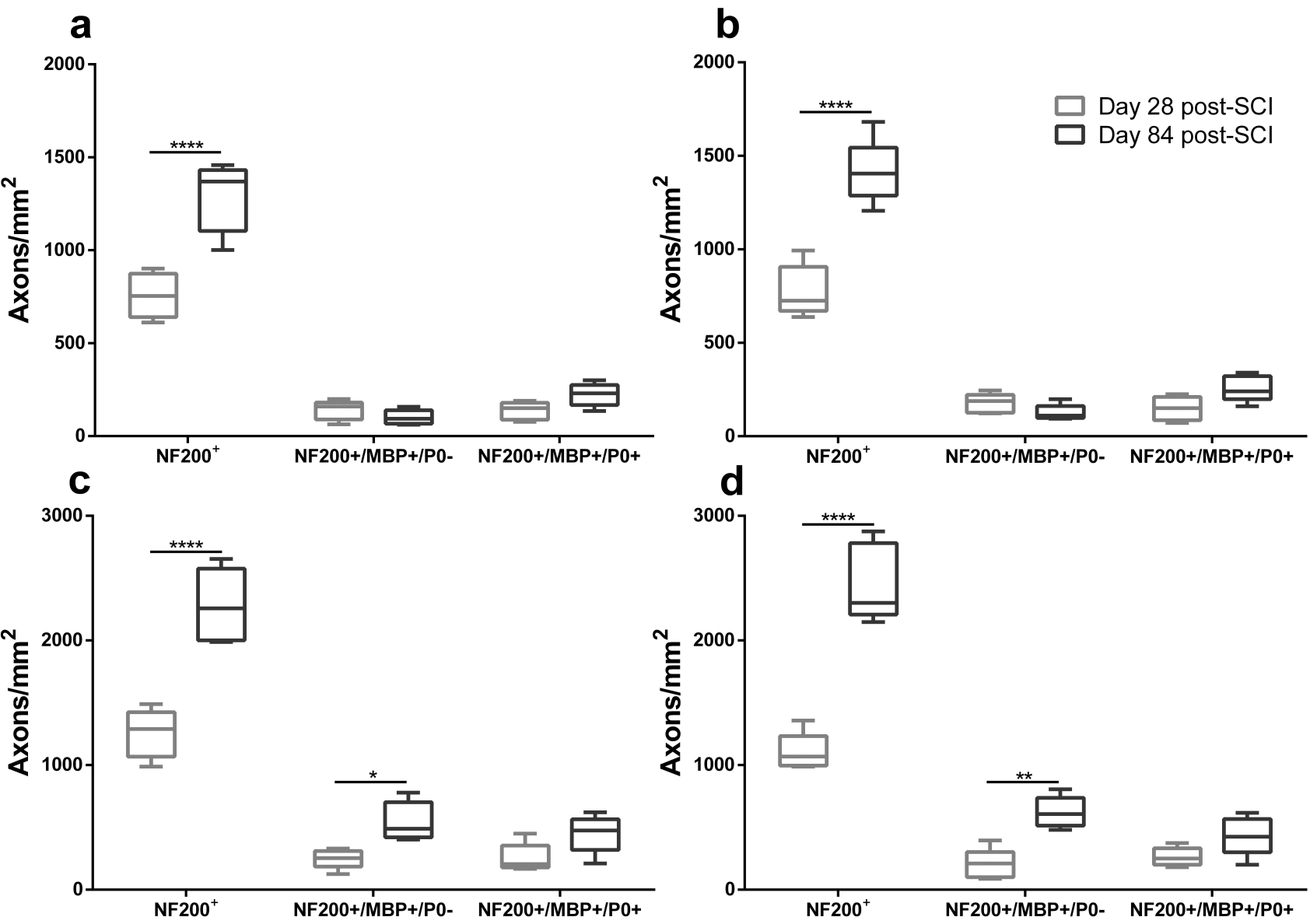
a
b
c
d
Axons/mm2
2000
1500
1000
500
0
3000
****
*
**
Day 28 post-SCI
Day 84 post-SCI
NF200+
NF200+/MBP+/P0-
NF200+/MBP+/P0+

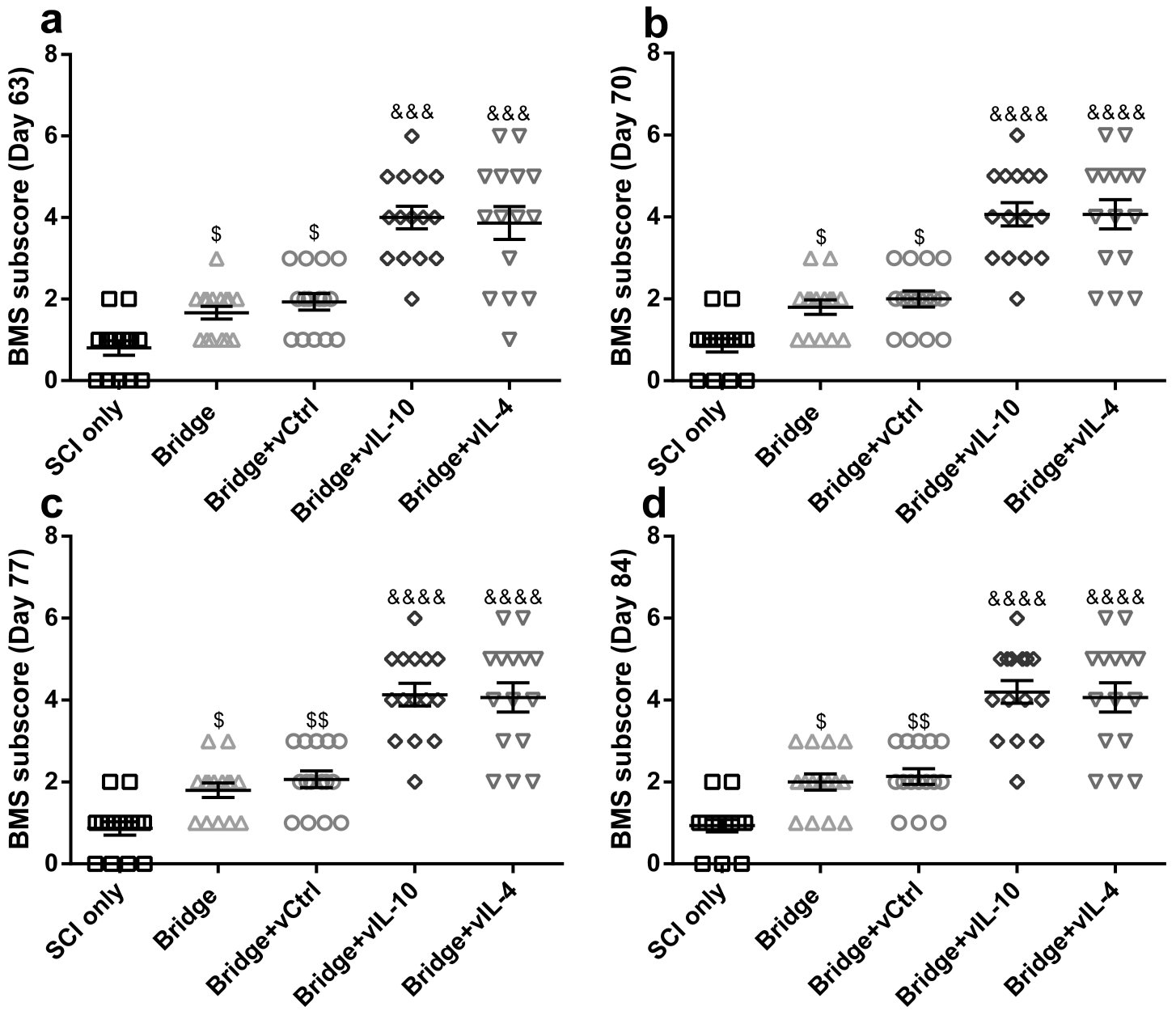
a
BMS subscore (Day 63)
8
6
4
2
0
&&&
&&&
$
$
SCI only
Bridge
Bridge+vCtrl
Bridge+vIL-10
Bridge+vIL-4
b
BMS subscore (Day 70)
&&&&
&&&&
$
$
c
BMS subscore (Day 77)
&&&&
&&&&
$
$$
d
BMS subscore (Day 84)
&&&&
&&&&
$
$$

Supplemental figure legends

Figure. S1. PLG multichannel bridge and hemi-sectional SCI model. (a) Photomicrograph of a bridge with 200 μm multichannel. (b) Schematic representation of hemi-section SCI at T9-T10 and multichannel bridge implantation in the injury site. Illustrating approximate bridge dimensions. (c) Schematic multichannel bridge regions where the bridge was divided for analysis. From the rostral edge of the bridge/tissue interface, rostral region analysis was done at 300 μm, middle at 900 μm, and caudal at 1600 μm.

Figure. S2. Local delivery of anti-inflammatory cytokine lentiviral vectors alters (a) Leukocyte activation (GO:0045321)-, (b) Inflammatory response (GO:0006954)-, (c) Leukocyte migration (GO:0002685)-, (d) Immune response (GO:0006955)- (e) Neuron differentiation (GO:0030182)- and (f) Synapse organization (GO:0050808)-related gene ontologies at day 7 post-SCI.

Figure. S3. Overexpression of anti-inflammatory cytokines influences the number of M2 phenotypes within the bridges. (a) The transgene expression of IL-10 was associated with the increased number of M2 phenotypes (Pearson coefficient=0.9093; $P<0.0001$; $r^2=0.8268$). (b) Overexpression of IL-4 also correlated to increased number of M2 macrophages at the injury site (Pearson coefficient=0.7067; $P=0.0032$; $r^2=0.4994$).

Figure. S4. In the sub-acute phase, extensive co-localization of MBP^+ and $P0^+$ myelin was observed around and outer surface of multichannel bridges in the rostral position for (a) vIL-10 and (b) vIL-4 (scale bar 50 μm). The dashed lines indicate the interface between bridge implants and spinal cord tissue. (c) Percentage of axons that were myelinated within the bridge area at day 28 post-SCI. No difference was observed between groups. One-way ANOVA with Tukey's post hoc test (mean±SEM, n=5/group).

Figure. S5. vIL-10 and vIL-4 delivery increases the number of axons and oligodendrocyte-derived myelinated axons as a function of time at the injury. The total number of axons, oligodendrocyte-derived and Schwann cell-derived myelinated axons were quantified in delivery of (a) bridge only, (b) vCtrl, (c) vIL-10, and (d) vIL-4 in the sub-acute (day 28) and chronic phase (day 84). The statistical tests were completed using a two-way ANOVA with Šidák correction for the multiple comparisons. (*$P<0.05$, **$P<0.01$ and ****$P<0.0001$, n=5/group)

Figure. S6. Multichannel bridge with anti-inflammatory cytokines improves specific components of locomotion recovery from SCI. (a-d) The BMS subscore in vIL-4 and vIL-10 groups was significantly increased relative to bridge only and vCtrl throughout day 84. Furthermore, bridge itself increased the frequency of plantar stepping and fore limb-hind limb coordination compared to SCI only as a function of time. Statistical test was completed using a one-way ANOVA with Tukey's post hoc test. $^{\$}P<0.05$, and $^{\$\$}P<0.01$ compared to SCI only, and $^{\&\&\&}P<0.001$ and $^{\&\&\&\&}P<0.0001$ compared to vCtrl; mean±SEM and n=15/group

Table S1. Gene ontology accession number

Name	Accession Number
Inflammatory response	GO:0006954
Leukocyte activation	GO:0045321
Nervous system development	GO:0007399
Locomotor behavior	GO:0007626
Synapse organization	GO:0050808
Immune system process	GO:0002682
Leukocyte migration	GO:0002685
Immune response	GO:0006955
Neuron differentiation	GO:0030182
Chemical synaptic transmission	GO:0007268

Table S2. Primer sequences for qRT-PCR

Gene	Accession number (GenBank)	Forward (5'-3')	Reverse (5'-3')
Il7r	NM_008372.4	GCTGTACACAGTGCAAACCG	GTGGAGATGGGCTGTCTCTG
Cd28	NM_007642.4	TGGCTTGCTAGTGACAGTGG	CATTGGTGGCCCAGTAGAGG
Cdk6	NM_009873.3	GCATCGTGATCTGAAACCGC	CCACGTCTGAACTTCCACGA
Arginase1	U51805.1	GAACACGGCAGTGGCTTTAAC	TGCTTAGCTCTGTCTGCTTTGC
CD206	NM_008625.2	TCTTTGCCTTTCCCAGTCTCC	TGACACCCAGCGGAATTTC
Retnla	NM_020509.3	GGTCCCAGTGCATATGGATGAGACCATAGA	CACCTCTTCACTCGAGGGACAGTTGGCAGC
CD86	NM_019388.3	TTGTGTGTGTTCTGGAAACGGAG	AACTTAGAGGCTGTGTTGCTGGG
iNOS	U58677.1	CCCTTCAATGGTTGGTACATGG	ACATTGATCTCCGTGACAGCC
MHC-II	NM_207105.3	GACGCTCAACTTGTCCCAAAAC	GCAGCCGTGAACTTGTTGAAC
18s-rRNA	NR_003278.3	GCAATTATTCCCCATGAACG	GGCCTCACTAAACCATCCAA-3
Hoxc10	NM_010462.5	TGTACAGTGCAGAGAAGCGG	GTGTCTGGACTGGAGTCTGC
Chat	NM_009891.2	GGCTTTTGTGCAAGCCATGA	CACAGGGCCATAACAGCAGA
Efna3	NM_010108.1	CTACATCTCCACGCCCACTC	CCTGGGGATTCTCTCCCTCA
Hapln4	NM_177900.4	GGTCACAAGATGATCGTGCC	TGACCTTAAGAAGCCGAGCA
Trpc5	NM_009428.3	AACTCCCTCTACCTGGCAAC	TTCTGCAATCAGAGTCGGGT
Lhx5	NM_008499.5	CAGGATCCGTTACAGGACGA	AACCACACCTGAATGACCCT
Scn1a	NM_001313997.1	GTGTGCTCAAGCTCATCTCG	GCACCTTTGATCAGGCGTAG
Hoxd10	NM_013554.5	AACCAGCAATTGGCTCACTG	TTACTGATCTCTAGGCGGCG
Negr1	NM_177274.4	CGGTGCTCAGGTGTTACTTG	GAAACTCGAGGGTCCACTGA